Multilayered Media Green's Functions in Integral Equation Formulations

Krzysztof A. Michalski* and Juan R. Mosig†

Abstract—A compact representation is given of the electric- and magnetic-type dyadic Green's functions for plane-stratified, multilayered uniaxial media, based on the transmission-line network analog along the axis normal to the stratification. Furthermore, mixed-potential integral equations are derived within the framework of this transmission-line formalism for arbitrarily shaped, conducting or penetrable objects embedded in the layered medium. Although the development emphasizes laterally unbounded environments, an extension to the case of a medium enclosed by a rectangular shield is also included.

I Introduction

In a variety of applications, such as geophysical prospecting [1–3], remote sensing [4], wave propagation [5, 6], and microstrip circuits and antennas [7–9], it is necessary to compute the electromagnetic field in a layered medium. For a given set of sources, the field may easily be found if the dyadic Green's functions (DGFs) of the environment are available. Numerous authors have derived DGFs for layered media, both isotropic and anisotropic [10–29]. Most of the recent developments in this area have been driven by applications to microstrip patch antennas, printed circuit boards, and monolithic microwave/millimeter-wave integrated circuits.

When the currents are not known *a priori*, which is usually the case in scattering and antenna problems, the DGFs may be used to formulate integral equations for the true or equivalent currents, which are then solved numerically by the method of moments (MOM) [30]. The hypersingular behavior of some of the integral equation kernels causes difficulties in the solution procedure [31], which may be avoided if the fields are expressed in terms of vector and scalar potentials with weakly singular kernels. This led to the development of *mixed-potential integral equations* (MPIEs) for arbitrarily shaped scatterers in free space [32–35]. In layered media, an important advantage of the MPIEs is that the spectral Sommerfeld-type integrals (or series, in the case of laterally shielded environments) appearing in the potential kernels converge more rapidly and are easier to accelerate than those associated with the field forms, which are in effect obtained by differentiation of the potentials. This

*Electromagnetics & Microwave Laboratory, Department of Electrical Engineering, Texas A&M University, College Station, Texas 77843–3128, USA

†Laboratory of Electromagnetics and Acoustics, Swiss Federal Institute of Technology, EPFL–Ecublens, CH–1015 Lausanne, Switzerland

was recognized early on by Mosig and Gardiol [36–38], who derived and successfully applied an MPIE for planar microstrip structures on a grounded substrate. This MPIE could not easily be extended to general non-planar conductors, because—as was later realized—in layered media the scalar potential kernels associated with horizontal and vertical current components were different [39, 40].However, ways to handle vertical probe feeds were soon devised, incorporating both the 'horizontal' and 'vertical' scalar potential kernels [41–44]. Since different scalar potential kernels were used for the horizontal and vertical currents, a fictitious point charge had to be introduced at the feed point. Other two-potential MPIE formulations were also proposed to tackle vertical probes [45, 46]. The development of efficient procedures for the computation of the Sommerfeld integrals [36] and an extension to multilayered media [42] made the MPIE an attractive approach for planar microstrip circuit and antenna problems [47–57].

To tackle arbitrarily shaped, three-dimensional conducting objects, Michalski [39] proposed to use the 'horizontal' scalar potential kernel throughout, which necessitated a proper 'correction' of those elements of the dyadic vector potential kernel associated with the vertical current component. This approach was later put on firmer theoretical basis by Michalski and Zheng [58], who described three distinct MPIE formulations (referred to as A, B, and C) for multilayered media and discussed their relative merits. One of these MPIEs (formulation C), which was deemed preferable for objects penetrating an interface, was implemented and validated for the case of a two-layer medium [59]. Furthermore, the MPIE of Mosig and Gardiol and other previously used MPIEs [60–62] were classified as special cases of the newly developed formulations. The formulation C MPIE was later applied to microstrip transmission lines of arbitrary cross-section [63], vertical probe fed microstrip patch antennas [64], arbitrarily shaped microstrip patch resonators in uniaxial substrates [65], and printed spiral antennas [66]. Recently, modified MPIEs were proposed, in which the scalar potential, rather than the vector potential kernel, is 'corrected' [67–69]. Alternative derivations of the three MPIE formulations for multilayered uniaxial media were also presented [70, 71]. More recently, the formulation C MPIE was adopted to analyze electromagnetic scattering by wires [72] and conducting bodies of revolution [73, 74] buried in earth.

In this paper, we present a compact formulation of the electric- and magnetic-type DGFs for plane-stratified, multilayered uniaxial media, based on the transmission-line network analog along the axis normal to the stratification [75]. Furthermore, we derive within the framework of this transmission-line formalism MPIEs for arbitrarily shaped, penetrable or conducting objects embedded in the multilayered medium. Attention is limited to media with at most uniaxial anisotropy, which while being important in practice [76–78], still allow the simple transmission-line representation of the electromagnetic fields. The emphasis is on laterally unbounded environments, but an extension to the case of a layered medium enclosed by a rectangular shield is also included.

In Section II, which provides the motivation for the following development, the formulation of the integral equations for penetrable or perfectly conducting objects embedded in a layered medium is discussed. In particular, the MPIEs are introduced. In Section III, the Fourier transform formalism is introduced and the spectral fields are expressed in terms of the voltages and currents on the transmission-line analog of the medium. In Section IV, the DGFs for a medium with an as yet unspecified stratification are expressed in terms of the transmission-line Green's functions (TLGFs). In Section V, two alternative MPIE forms are

derived, with the kernels expressed in terms of the TLGFs, and their properties discussed. These MPIEs are applicable to arbitrarily shaped, three-dimensional objects, which may penetrate interfaces between dissimilar media. In Section VI, a practical algorithm is given for the efficient computation of the TLGFs for multilayered media with piecewise-constant parameters. Some important issues encountered in the computation of the Sommerfeld integrals are discussed in Section VII. In particular, the quasi-static forms of the MPIE kernels are derived. In Section VIII, the formulation is extended to the practically important case of a medium shielded by a rectangular enclosure. The material presented in Sections IX and X is relevant to scattering and radiation problems involving objects in multilayered media not shielded from above. In Section IX, the far-zone DGFs are derived and a simple procedure for the computation of the radiation field is presented. In Section X, the field excited in the multilayered medium by a plane-wave is expressed in terms of the TLGFs.

The $e^{j\omega t}$ time dependence is implicit in the formulation and the stratification is assumed to be transverse to the z-axis of the Cartesian (x, y, z)-coordinate system. Source coordinates are distinguished by primes, vectors are denoted by boldface letters, unit vectors are distinguished by carets, and dyadics are denoted by doubly underlined boldface letters.

II Formulation of Integral Equations

Consider an arbitrarily shaped object embedded in a layered medium and excited by known electric and magnetic currents $(\boldsymbol{J}^i, \boldsymbol{M}^i)$, as illustrated in Fig. 1(a). The equations governing the resulting electric and magnetic fields $(\boldsymbol{E}, \boldsymbol{H})$ are most easily derived by use of the equivalence principle [79, p. 106]. An external equivalent problem is shown in Fig. 1(b), where the surface currents $(\boldsymbol{J}_s, \boldsymbol{M}_s)$ and the *impressed* currents $(\boldsymbol{J}^i, \boldsymbol{M}^i)$ radiating in the layered medium produce the correct fields $(\boldsymbol{E}, \boldsymbol{H})$ exterior to S and null fields inside S. Clearly, $(\boldsymbol{E}, \boldsymbol{H}) = (\boldsymbol{E}^i + \boldsymbol{E}^s, \boldsymbol{H}^i + \boldsymbol{H}^s)$, where $(\boldsymbol{E}^i, \boldsymbol{H}^i)$ are the *impressed* fields due to $(\boldsymbol{J}^i, \boldsymbol{M}^i)$ and $(\boldsymbol{E}^s, \boldsymbol{H}^s)$ are the *scattered* fields due to $(\boldsymbol{J}_s, \boldsymbol{M}_s)$. The boundary conditions at S dictate that

$$\boldsymbol{M}_s = -\hat{\boldsymbol{n}} \times \left(\boldsymbol{E}^i + \boldsymbol{E}^s[\boldsymbol{J}_s, \boldsymbol{M}_s]\right)_{S_+} \tag{1}$$

$$\boldsymbol{J}_s = \hat{\boldsymbol{n}} \times \left(\boldsymbol{H}^i + \boldsymbol{H}^s[\boldsymbol{J}_s, \boldsymbol{M}_s]\right)_{S_+} \tag{2}$$

where $\hat{\boldsymbol{n}}$ is the outward unit vector normal to S, and where the subscript S_+ indicates that the fields are evaluated as the observation point approaches S from the exterior region. In linear media the fields due to arbitrary current distributions $(\boldsymbol{J}, \boldsymbol{M})$ may be expressed as

$$\boldsymbol{E} = \langle \underline{\underline{\boldsymbol{G}}}^{EJ}; \boldsymbol{J} \rangle + \langle \underline{\underline{\boldsymbol{G}}}^{EM}; \boldsymbol{M} \rangle \tag{3}$$

$$\boldsymbol{H} = \langle \underline{\underline{\boldsymbol{G}}}^{HJ}; \boldsymbol{J} \rangle + \langle \underline{\underline{\boldsymbol{G}}}^{HM}; \boldsymbol{M} \rangle \tag{4}$$

where $\underline{\underline{\boldsymbol{G}}}^{PQ}(\boldsymbol{r}|\boldsymbol{r}')$ is the DGF relating P-type fields at $\boldsymbol{r}$ and Q-type currents at $\boldsymbol{r}'$. The notation $\langle , \rangle$ is used for integrals of products of two functions separated by the comma over their common spatial support, with a dot over the comma indicating a dot product. Since the DGFs for the layered medium of Fig. 1(b) are available—see Section IV, one can use (3)-(4) to compute the impressed fields and to express the scattered fields in (1)-(2) in terms of the unknown currents $(\boldsymbol{J}_s, \boldsymbol{M}_s)$. As a result, a set of two integral equations is obtained, which

may be solved for $(\boldsymbol{J}_s, \boldsymbol{M}_s)$. Once the latter are found, the scattered fields may be computed from (3)-(4).

In view of the hypersingular behavior of $\underline{\underline{\boldsymbol{G}}}^{EJ}$ and $\underline{\underline{\boldsymbol{G}}}^{HM}$, it is preferable to convert (3)-(4) into their mixed-potential forms. In this process, one encounters the previously mentioned dilemma caused by the fact that in layered media the scalar potential kernels associated with the horizontal and vertical current components are in general different [40]. Consequently, either the scalar or the vector potential kernel must be modified for arbitrary current distributions. We show in Section V that choosing the former route [67, 68] leads to the mixed-potential forms

$$\begin{aligned}\boldsymbol{E} = &-j\omega\mu_0\langle\underline{\underline{\boldsymbol{G}}}^{A};\boldsymbol{J}\rangle \\ &+\frac{1}{j\omega\epsilon_0}\nabla\left(\langle K^{\Phi},\nabla'\cdot\boldsymbol{J}\rangle+\langle C^{\Phi}\hat{\boldsymbol{z}};\boldsymbol{J}\rangle\right)+\langle\underline{\underline{\boldsymbol{G}}}^{EM};\boldsymbol{M}\rangle\end{aligned} \tag{5}$$

$$\begin{aligned}\boldsymbol{H} = &\langle\underline{\underline{\boldsymbol{G}}}^{HJ};\boldsymbol{J}\rangle-j\omega\epsilon_0\langle\underline{\underline{\boldsymbol{G}}}^{F};\boldsymbol{M}\rangle \\ &+\frac{1}{j\omega\mu_0}\nabla\left(\langle K^{\Psi},\nabla'\cdot\boldsymbol{M}\rangle+\langle C^{\Psi}\hat{\boldsymbol{z}};\boldsymbol{M}\rangle\right)\end{aligned} \tag{6}$$

where μ_0 and ϵ_0 denote the free-space permeability and permittivity, respectively, and the prime over the operator nabla indicates that the derivatives are with respect to the source coordinates. Furthermore, $\underline{\underline{\boldsymbol{G}}}^{A}$ and $\underline{\underline{\boldsymbol{G}}}^{F}$ are the DGFs for the magnetic and electric vector potentials, respectively, K^{Φ} and K^{Ψ} are the corresponding scalar potential kernels, and C^{Φ} and C^{Ψ} are the *correction factors* associated with the longitudinal electric and magnetic currents, respectively [58]. Note that $\nabla\cdot\boldsymbol{J}$ and $\nabla\cdot\boldsymbol{M}$ are proportional to, respectively, the electric and magnetic charge densities. As also shown in Section V, the correction terms in (5)-(6) may be grouped with the vector potential terms, resulting in the more conventional mixed-potential forms

$$\boldsymbol{E} = -j\omega\mu_0\langle\underline{\underline{\boldsymbol{K}}}^{A};\boldsymbol{J}\rangle+\frac{1}{j\omega\epsilon_0}\nabla\langle K^{\Phi},\nabla'\cdot\boldsymbol{J}\rangle+\langle\underline{\underline{\boldsymbol{G}}}^{EM};\boldsymbol{M}\rangle \tag{7}$$

$$\boldsymbol{H} = \langle\underline{\underline{\boldsymbol{G}}}^{HJ};\boldsymbol{J}\rangle-j\omega\epsilon_0\langle\underline{\underline{\boldsymbol{K}}}^{F};\boldsymbol{M}\rangle+\frac{1}{j\omega\mu_0}\nabla\langle K^{\Psi},\nabla'\cdot\boldsymbol{M}\rangle \tag{8}$$

where $\underline{\underline{\boldsymbol{K}}}^{A}$ and $\underline{\underline{\boldsymbol{K}}}^{F}$ are the modified vector potential kernels [39, 58]. When only transverse currents are present, which is an assumption often made in the analysis of planar microstrip structures, the mixed-potential forms (5)-(6) and (7)-(8) become identical.

Equations (1)-(2) are usually enforced in the weak sense by *testing* them with a set of linearly independent vector functions $\{\boldsymbol{\Lambda}_k\}$ tangential to S. When the mixed-potential representations (7)-(8) are used in the weak forms of (1)-(2) to express the scattered fields radiated by $(\boldsymbol{J}_s, \boldsymbol{M}_s)$, one obtains the MPIEs

$$\begin{aligned}-\langle\hat{\boldsymbol{n}}\times\boldsymbol{\Lambda}_k;\boldsymbol{M}_s\rangle = &\langle\boldsymbol{\Lambda}_k;\boldsymbol{E}^i\rangle-j\omega\mu_0\langle\boldsymbol{\Lambda}_k;\langle\underline{\underline{\boldsymbol{K}}}^{A};\boldsymbol{J}_s\rangle\rangle \\ &-\frac{1}{j\omega\epsilon_0}\langle\nabla\cdot\boldsymbol{\Lambda}_k,\langle K^{\Phi},\nabla'\cdot\boldsymbol{J}_s\rangle\rangle+\langle\boldsymbol{\Lambda}_k;\langle\underline{\underline{\boldsymbol{G}}}^{EM};\boldsymbol{M}_s\rangle\rangle-\frac{1}{2}\langle\boldsymbol{\Lambda}_k;\boldsymbol{M}_s\times\hat{\boldsymbol{n}}\rangle\end{aligned} \tag{9}$$

$$\begin{aligned}\langle\hat{\boldsymbol{n}}\times\boldsymbol{\Lambda}_k;\boldsymbol{J}_s\rangle = &\langle\boldsymbol{\Lambda}_k;\boldsymbol{H}^i\rangle+\langle\boldsymbol{\Lambda}_k;\langle\underline{\underline{\boldsymbol{G}}}^{HJ};\boldsymbol{J}_s\rangle\rangle-\frac{1}{2}\langle\boldsymbol{\Lambda}_k;\hat{\boldsymbol{n}}\times\boldsymbol{J}_s\rangle \\ &-j\omega\epsilon_0\langle\boldsymbol{\Lambda}_k;\langle\underline{\underline{\boldsymbol{K}}}^{F};\boldsymbol{M}_s\rangle\rangle-\frac{1}{j\omega\mu_0}\langle\nabla\cdot\boldsymbol{\Lambda}_k,\langle K^{\Psi},\nabla'\cdot\boldsymbol{M}_s\rangle\rangle\end{aligned} \tag{10}$$

in which the derivatives of the scalar potentials have been transferred onto the testing functions by means of the Gauss' theorem [80, p. 503]. Also, principal parts have been extracted from the integrals involving the kernels $\underline{\underline{\boldsymbol{G}}}^{EM}$ and $\underline{\underline{\boldsymbol{G}}}^{HJ}$ in the limit as the observation point approaches S from the outside [81]. Note that additional terms will appear in (9)-(10) when (5)-(6) are employed in place of (7)-(8).

The first of the MPIEs (9)-(10) is also referred to as the electric field integral equation (EFIE), and the second as the magnetic field integral equation (MFIE). Only the EFIE is applicable to open shells made of a perfect electric conductor (PEC). For closed PEC objects, $\boldsymbol{M}_s = \boldsymbol{0}$ and either the EFIE, or the MFIE, or their combination known as the combined field integral equation (CFIE), may be used to solve for $\boldsymbol{J}_s$. The CFIE does not suffer from the internal resonance problems that plague the EFIE and the MFIE [82]. Nonperfect conductors can often be modeled as surface impedance objects characterized by the condition $\boldsymbol{M}_s = Z_s \boldsymbol{J}_s \times \hat{\boldsymbol{n}}$, where Z_s is the skin effect surface impedance [83, 84]. One can use this impedance boundary condition to eliminate $\boldsymbol{M}_s$ from (9)-(10) and to solve either the EFIE, or the MFIE, or the CFIE for $\boldsymbol{J}_s$. In the analysis of microstrip structures, it is common to use a simplified form of the EFIE, which neglects the contribution of $\boldsymbol{M}_s$ to $\boldsymbol{E}^s$ [85].

The treatment of penetrable objects depends on whether they are homogeneous of not. In the former case, an interior equivalent problem is constructed, in which the surface currents $(-\boldsymbol{J}_s, -\boldsymbol{M}_s)$ radiating in an unbounded space filled with the medium of the object produce the correct fields $(\boldsymbol{E}, \boldsymbol{H})$ inside S and null fields outside. This leads to equations of the same form as (9)-(10), except that the homogeneous medium Green's functions are used. Combining these equations with those for the exterior problem yields a coupled set of MPIEs uniquely solvable for $(\boldsymbol{J}_s, \boldsymbol{M}_s)$ [86]. The principal parts arising from the interior and exterior problems cancel out in this case. For inhomogeneous objects, DGFs associated with the interior equivalent problem are not available and (9)-(10) must be augmented by the weak form of a differential equation governing the fields inside the volume enclosed by S. This leads to a set of hybrid integro-differential equations for $(\boldsymbol{J}_s, \boldsymbol{M}_s)$ and the fields inside the objects [87–90]. One advantage of this approach is that upon discretization the differential equation leads to a sparsely populated submatrix, which may be exploited to reduce the computational effort involved in the solution of the hybrid system. An alternative procedure, applicable to both homogeneous and inhomogeneous objects, is to replace the object in the interior equivalent problem with electric and magnetic volume polarization currents radiating in free space [34, 79, p. 126]. As a result, a set of hybrid volume-surface integral equations is obtained [91]. An advantage of this approach is that—unlike in the standard domain integral equation methods [21, 25]—there are no Sommerfeld integrals associated with the interior problem.

There are important applications where the object in Fig. 1(a) is excited through an aperture in a conducting ground plane. In such cases the aperture is 'shorted' and an equivalent magnetic surface current is placed over the shorted region to support the correct electric field there. The contribution of this current is then be added to the MPIEs (9)-(10). Since the equivalent aperture current is typically unknown, the MPIEs are supplemented by an integral equation obtained by enforcing the continuity of the tangential magnetic field across the aperture [92].

Apart from the dyadic nature of the vector potential kernels, the MPIEs (9)-(10) have the same form as their free-space counterparts and thus are amenable to the well-established

numerical solution procedures developed for the latter [32, 33, 35, 84, 93]. The basic step in these procedures, which are variations of the MOM, is the expansion of $(\boldsymbol{J}_s, \boldsymbol{M}_s)$ in terms of a set of vector basis functions, where the latter may or may not be the same as the testing functions $\{\boldsymbol{\Lambda}_k\}$. As a result, the MPIEs (9)-(10) are converted into matrix equations for the current expansion coefficients, which may be solved by standard techniques.

III Scalarization of Maxwell's Equations

Consider a uniaxially anisotropic, possibly lossy medium, which is transversely unbounded with respect to the z-axis and is characterized, relative to free space, by z-dependent, in general complex-valued permeability and permittivity dyadics, $\underline{\underline{\boldsymbol{\mu}}} = \underline{\underline{\boldsymbol{I}}}_t \mu_t + \hat{\boldsymbol{z}}\hat{\boldsymbol{z}}\mu_z$ and $\underline{\underline{\boldsymbol{\epsilon}}} = \underline{\underline{\boldsymbol{I}}}_t \epsilon_t + \hat{\boldsymbol{z}}\hat{\boldsymbol{z}}\epsilon_z$, respectively, where $\underline{\underline{\boldsymbol{I}}}_t$ is the transverse unit dyadic. We wish to compute the fields $(\boldsymbol{E}, \boldsymbol{H})$ at an arbitrary point $\boldsymbol{r}$ due to a specified current distribution $(\boldsymbol{J}, \boldsymbol{M})$, as illustrated in Fig. 2(a). These fields are governed by the Maxwell's equations [75, p. 745]

$$\nabla \times \boldsymbol{E} = -j\omega\mu_0 \underline{\underline{\boldsymbol{\mu}}} \cdot \boldsymbol{H} - \boldsymbol{M}, \quad \nabla \times \boldsymbol{H} = j\omega\epsilon_0 \underline{\underline{\boldsymbol{\epsilon}}} \cdot \boldsymbol{E} + \boldsymbol{J} \tag{11}$$

Since the medium is homogeneous and of infinite extent in any transverse (to z) plane, the analysis is facilitated by the Fourier transformation of all fields with respect to the transverse coordinates. Hence, we express any scalar field component as $f(\boldsymbol{r}) \equiv f(\boldsymbol{\rho}; z)$, where $\boldsymbol{\rho} = \hat{\boldsymbol{x}}x + \hat{\boldsymbol{y}}y$ is the projection of $\boldsymbol{r}$ on the (x, y)-plane, and introduce the Fourier transform pair

$$\mathcal{F}f(\boldsymbol{r}) \equiv \tilde{f}(\boldsymbol{k}_\rho; z) = \int_{-\infty}^{+\infty}\int_{-\infty}^{+\infty} f(\boldsymbol{r}) e^{j\boldsymbol{k}_\rho \cdot \boldsymbol{\rho}}\, dxdy \tag{12}$$

$$\mathcal{F}^{-1}\tilde{f}(\boldsymbol{k}_\rho; z) \equiv f(\boldsymbol{r}) = \frac{1}{(2\pi)^2}\int_{-\infty}^{+\infty}\int_{-\infty}^{+\infty} \tilde{f}(\boldsymbol{k}_\rho; z) e^{-j\boldsymbol{k}_\rho \cdot \boldsymbol{\rho}}\, dk_x dk_y \tag{13}$$

where $\boldsymbol{k}_\rho = \hat{\boldsymbol{x}}k_x + \hat{\boldsymbol{y}}k_y$. Upon applying (12) to (11) and separating the transverse and longitudinal parts of the resulting equations, one obtains

$$\frac{d}{dz}\tilde{\boldsymbol{E}}_t = \frac{1}{j\omega\epsilon_0\epsilon_t}(k_t^2 - \nu^e \boldsymbol{k}_\rho \boldsymbol{k}_\rho \cdot)(\tilde{\boldsymbol{H}}_t \times \hat{\boldsymbol{z}}) + \boldsymbol{k}_\rho \frac{\tilde{J}_z}{\omega\epsilon_0\epsilon_z} - \tilde{\boldsymbol{M}}_t \times \hat{\boldsymbol{z}} \tag{14}$$

$$\frac{d}{dz}\tilde{\boldsymbol{H}}_t = \frac{1}{j\omega\mu_0\mu_t}(k_t^2 - \nu^h \boldsymbol{k}_\rho \boldsymbol{k}_\rho \cdot)(\hat{\boldsymbol{z}} \times \tilde{\boldsymbol{E}}_t) + \boldsymbol{k}_\rho \frac{\tilde{M}_z}{\omega\mu_0\mu_z} - z \times \tilde{\boldsymbol{J}}_t \tag{15}$$

$$-j\omega\epsilon_0\epsilon_z\tilde{E}_z = j\boldsymbol{k}_\rho \cdot (\tilde{\boldsymbol{H}}_t \times \hat{\boldsymbol{z}}) + \tilde{J}_z \tag{16}$$

$$-j\omega\mu_0\mu_z\tilde{H}_z = j\boldsymbol{k}_\rho \cdot (\hat{\boldsymbol{z}} \times \tilde{\boldsymbol{E}}_t) + \tilde{M}_z \tag{17}$$

where $k_t = k_0\sqrt{\mu_t\epsilon_t}$, $k_0 = \omega\sqrt{\mu_0\epsilon_0}$ being the free-space wavenumber, and where $\nu^e = \epsilon_t/\epsilon_z$ and $\nu^h = \mu_t/\mu_z$ are referred to as, respectively, the electric and magnetic anisotropy ratios. The subsequent analysis is greatly simplified if one defines a rotated spectrum-domain coordinate system based on $(\boldsymbol{k}_\rho, \hat{\boldsymbol{z}} \times \boldsymbol{k}_\rho)$ (see Fig. 3), with the unit vectors $(\hat{\boldsymbol{u}}, \hat{\boldsymbol{v}})$ given by [94]

$$\hat{\boldsymbol{u}} = \frac{k_x}{k_\rho}\hat{\boldsymbol{x}} + \frac{k_y}{k_\rho}\hat{\boldsymbol{y}}, \quad \hat{\boldsymbol{v}} = -\frac{k_y}{k_\rho}\hat{\boldsymbol{x}} + \frac{k_x}{k_\rho}\hat{\boldsymbol{y}} \tag{18}$$

where $k_\rho = \sqrt{k_x^2 + k_y^2}$. If we now express the transverse electric and magnetic fields as

$$\tilde{\boldsymbol{E}}_t = \hat{\boldsymbol{u}} V^e + \hat{\boldsymbol{v}} V^h \,, \quad \tilde{\boldsymbol{H}}_t \times \hat{\boldsymbol{z}} = \hat{\boldsymbol{u}} I^e + \hat{\boldsymbol{v}} I^h \tag{19}$$

and project (14)-(15) on $\hat{\boldsymbol{u}}$ and $\hat{\boldsymbol{v}}$, we find that these equations decouple into two sets of transmission line equations of the form

$$\frac{dV^p}{dz} = -jk_z^p Z^p I^p + v^p \,, \quad \frac{dI^p}{dz} = -jk_z^p Y^p V^p + i^p \tag{20}$$

where the superscript p assumes the values of e or h. Hence, the components of $\tilde{\boldsymbol{E}}_t$ and $\tilde{\boldsymbol{H}}_t$ in the (u, v)-plane may be interpreted as voltages and currents on a transmission-line analog of the medium along the z-axis—which was anticipated in the notation introduced in (19). The propagation wavenumbers and the characteristic impedances and admittances of this transmission line are given as

$$k_z^p = \sqrt{k_t^2 - \nu^p k_\rho^2} \tag{21}$$

$$Z^e = \frac{1}{Y^e} = \frac{k_z^e}{\omega\epsilon_0\epsilon_t} \,, \quad Z^h = \frac{1}{Y^h} = \frac{\omega\mu_0\mu_t}{k_z^h} \tag{22}$$

where the square root branch in (21) is specified by the condition that $-\pi < \arg\{k_z^p\} \le 0$. The voltage and current sources in (20) are given by

$$v^e = \frac{k_\rho}{\omega\epsilon_0\epsilon_z}\tilde{J}_z - \tilde{M}_v \,, \quad i^e = -\tilde{J}_u \,,$$

$$i^h = -\frac{k_\rho}{\omega\mu_0\mu_z}\tilde{M}_z - \tilde{J}_v \,, \quad v^h = \tilde{M}_u \tag{23}$$

This relationship between the field sources and the transmission line sources is summarized in Table I. In view of (19) and (16)-(17), the spectral fields may now be expressed as

$$\tilde{\boldsymbol{E}} = \hat{\boldsymbol{u}} V^e + \hat{\boldsymbol{v}} V^h - \hat{\boldsymbol{z}} \frac{1}{j\omega\epsilon_0\epsilon_z}\left(jk_\rho I^e + \tilde{J}_z\right) \tag{24}$$

$$\tilde{\boldsymbol{H}} = -\hat{\boldsymbol{u}} I^h + \hat{\boldsymbol{v}} I^e + \hat{\boldsymbol{z}} \frac{1}{j\omega\mu_0\mu_z}\left(jk_\rho V^h - \tilde{M}_z\right) \tag{25}$$

which indicate that outside the source region (V^e, I^e) and (V^h, I^h) represent fields that are, respectively, transverse-magnetic (TM) and transverse-electric (TE) to z. The space domain fields $(\boldsymbol{E}, \boldsymbol{H})$ are obtained from (24)-(25) via the inverse transform (13).

The original vector problem of Fig. 2(a) has thus been reduced to the scalar transmission line problem of Fig. 2(b). Note that—since the superscript p represents e or h—two transmission lines are involved, associated, respectively, with the TM and TE partial fields. As Table I indicates, transverse electric or transverse magnetic currents always excite both the TM and TE transmission lines, while a longitudinal electric (magnetic) current only excites the TM (TE) transmission line.

IV Derivation of Dyadic Green's Functions

Consider the solutions of the transmission-line equations (20) for unit-strength impulsive sources. Hence, let $V_i^p(z|z')$ and $I_i^p(z|z')$ denote the voltage and current, respectively, at z due to a 1 A shunt current source at z', and let $V_v^p(z|z')$ and $I_v^p(z|z')$ denote the voltage and current, respectively, at z due to a 1 V series voltage source at z' (see Fig. 4). Then it follows from (20) that these TLGFs satisfy the equations

$$\frac{dV_i^p}{dz} = -jk_z^p Z^p I_i^p\,, \quad \frac{dI_i^p}{dz} = -jk_z^p Y^p V_i^p + \delta(z-z') \tag{26}$$

$$\frac{dV_v^p}{dz} = -jk_z^p Z^p I_v^p + \delta(z-z')\,, \quad \frac{dI_v^p}{dz} = -jk_z^p Y^p V_v^p \tag{27}$$

where δ is the Dirac delta, and that they possess the reciprocity properties [75, p. 194]

$$V_i^p(z|z') = V_i^p(z'|z)\,, \quad I_v^p(z|z') = I_v^p(z'|z)\,,$$

$$V_v^p(z|z') = -I_i^p(z'|z)\,, \quad I_i^p(z|z') = -V_v^p(z'|z) \tag{28}$$

The linearity of the transmission-line equations (20) allows one to obtain (V^p, I^p) at any point z via the superposition integrals

$$V^p = \langle V_i^p, i^p\rangle + \langle V_v^p, v^p\rangle\,, \quad I^p = \langle I_i^p, i^p\rangle + \langle I_v^p, v^p\rangle \tag{29}$$

Upon substituting these equations into (24)-(25) and using (23), one obtains spectrum-domain counterparts of (3)-(4), viz.,

$$\tilde{\boldsymbol{E}} = \langle \underline{\underline{\tilde{\boldsymbol{G}}}}^{EJ}; \tilde{\boldsymbol{J}}\rangle + \langle \underline{\underline{\tilde{\boldsymbol{G}}}}^{EM}; \tilde{\boldsymbol{M}}\rangle \tag{30}$$

$$\tilde{\boldsymbol{H}} = \langle \underline{\underline{\tilde{\boldsymbol{G}}}}^{HJ}; \tilde{\boldsymbol{J}}\rangle + \langle \underline{\underline{\tilde{\boldsymbol{G}}}}^{HM}; \tilde{\boldsymbol{M}}\rangle \tag{31}$$

where the spectral DGFs $\underline{\underline{\tilde{\boldsymbol{G}}}}^{PQ}(\boldsymbol{k}_\rho; z|z')$ are given as

$$\begin{aligned}\underline{\underline{\tilde{\boldsymbol{G}}}}^{EJ} = &-\hat{\boldsymbol{u}}\hat{\boldsymbol{u}}V_i^e - \hat{\boldsymbol{v}}\hat{\boldsymbol{v}}V_i^h + \hat{\boldsymbol{z}}\hat{\boldsymbol{u}}\frac{k_\rho}{\omega\epsilon_0\epsilon_z}I_i^e \\ &+ \hat{\boldsymbol{u}}\hat{\boldsymbol{z}}\frac{k_\rho}{\omega\epsilon_0\epsilon_z'}V_v^e + \hat{\boldsymbol{z}}\hat{\boldsymbol{z}}\frac{1}{j\omega\epsilon_0\epsilon_z'}\left[\frac{k_\rho^2}{j\omega\epsilon_0\epsilon_z}I_v^e - \delta(z-z')\right]\end{aligned} \tag{32}$$

$$\underline{\underline{\tilde{\boldsymbol{G}}}}^{HJ} = \hat{\boldsymbol{u}}\hat{\boldsymbol{v}}I_i^h - \hat{\boldsymbol{v}}\hat{\boldsymbol{u}}I_i^e - \hat{\boldsymbol{z}}\hat{\boldsymbol{v}}\frac{k_\rho}{\omega\mu_0\mu_z}V_i^h + \hat{\boldsymbol{v}}\hat{\boldsymbol{z}}\frac{k_\rho}{\omega\epsilon_0\epsilon_z'}I_v^e \tag{33}$$

$$\underline{\underline{\tilde{\boldsymbol{G}}}}^{EM} = -\hat{\boldsymbol{u}}\hat{\boldsymbol{v}}V_v^e + \hat{\boldsymbol{v}}\hat{\boldsymbol{u}}V_v^h + \hat{\boldsymbol{z}}\hat{\boldsymbol{v}}\frac{k_\rho}{\omega\epsilon_0\epsilon_z}I_v^e - \hat{\boldsymbol{v}}\hat{\boldsymbol{z}}\frac{k_\rho}{\omega\mu_0\mu_z'}V_i^h \tag{34}$$

$$\begin{aligned}\underline{\underline{\tilde{\boldsymbol{G}}}}^{HM} = &-\hat{\boldsymbol{u}}\hat{\boldsymbol{u}}I_v^h - \hat{\boldsymbol{v}}\hat{\boldsymbol{v}}I_v^e + \hat{\boldsymbol{z}}\hat{\boldsymbol{u}}\frac{k_\rho}{\omega\mu_0\mu_z}V_v^h \\ &+ \hat{\boldsymbol{u}}\hat{\boldsymbol{z}}\frac{k_\rho}{\omega\mu_0\mu_z'}I_i^h + \hat{\boldsymbol{z}}\hat{\boldsymbol{z}}\frac{1}{j\omega\mu_0\mu_z'}\left[\frac{k_\rho^2}{j\omega\mu_0\mu_z}V_i^h - \delta(z-z')\right]\end{aligned} \tag{35}$$

In the above, the primed media parameters are evaluated at the source coordinate z', and this convention is used throughout this paper. A convenient alternative form of $\underline{\underline{\tilde{G}}}^{EJ}$ is

$$\underline{\underline{\tilde{G}}}^{EJ} = -\underline{\underline{I}}_t V_i^h + \hat{\boldsymbol{u}}\hat{\boldsymbol{u}}\left(V_i^h - V_i^e\right) + \hat{\boldsymbol{z}}\hat{\boldsymbol{u}}\frac{k_\rho}{\omega\epsilon_0\epsilon_z} I_i^e + \hat{\boldsymbol{u}}\hat{\boldsymbol{z}}\frac{k_\rho}{\omega\epsilon_0\epsilon_z'} V_v^e + \hat{\boldsymbol{z}}\hat{\boldsymbol{z}}\frac{1}{j\omega\epsilon_0\epsilon_z'}\left[\frac{k_\rho^2}{j\omega\epsilon_0\epsilon_z} I_v^e - \delta(z-z')\right] \tag{36}$$

which is obtained from (32) by adding and subtracting $\hat{\boldsymbol{u}}\hat{\boldsymbol{u}}V_i^h$. Similar transformation may be applied to $\underline{\underline{\tilde{G}}}^{HM}$. It is also readily shown, using (28), that the spectral DGFs possess the reciprocity properties

$$\underline{\underline{\tilde{G}}}^{EJ}(\boldsymbol{k}_\rho; z|z') = \left[\underline{\underline{\tilde{G}}}^{EJ}(-\boldsymbol{k}_\rho; z'|z)\right]^T \tag{37}$$

$$\underline{\underline{\tilde{G}}}^{HM}(\boldsymbol{k}_\rho; z|z') = \left[\underline{\underline{\tilde{G}}}^{HM}(-\boldsymbol{k}_\rho; z'|z)\right]^T \tag{38}$$

$$\underline{\underline{\tilde{G}}}^{EM}(\boldsymbol{k}_\rho; z|z') = -\left[\underline{\underline{\tilde{G}}}^{HJ}(-\boldsymbol{k}_\rho; z'|z)\right]^T \tag{39}$$

where the superscript T indicates a transposed dyadics.

The spectral DGFs (32)-(35) may directly be used in integral equation formulations based on the spectral domain approach (SDA) [95–97]. The SDA and the space-domain integral equation technique are formally equivalent, and only differ in the order in which the spatial and spectral integrals are evaluated. However, the SDA is less flexible in terms of the geometries it can handle and less efficient than the space-domain MPIE [98].

The space-domain DGFs follow from (32)-(35) upon first projecting the unit vectors $(\hat{\boldsymbol{u}}, \hat{\boldsymbol{v}})$ on the (k_x, k_y)-coordinate system via (18) and then applying the inverse transformation (13). In view of the translational symmetry of the medium with respect to the transverse coordinates, we may write

$$\underline{\underline{G}}^{PQ}(\boldsymbol{r}|\boldsymbol{r}') \equiv \underline{\underline{G}}^{PQ}(\boldsymbol{\rho}-\boldsymbol{\rho}'; z|z') \tag{40}$$

where

$$\underline{\underline{G}}^{PQ}(\boldsymbol{\rho}; z|z') = \mathcal{F}^{-1}\underline{\underline{\tilde{G}}}^{PQ}(\boldsymbol{k}_\rho; z|z') \tag{41}$$

The spectral integrals that arise in (41) may be expressed as

$$\mathcal{F}^{-1}\left\{\begin{matrix}\sin\\ \cos\end{matrix} n\xi\, \tilde{f}(k_\rho)\right\} = (-j)^n \begin{matrix}\sin\\ \cos\end{matrix} n\varphi\; S_n\left\{\tilde{f}(k_\rho)\right\}, \quad n = 0, 1, 2 \tag{42}$$

where

$$S_n\left\{\tilde{f}(k_\rho)\right\} = \frac{1}{2\pi}\int_0^\infty \tilde{f}(k_\rho) J_n(k_\rho\rho) k_\rho\, dk_\rho \tag{43}$$

is referred to as a Sommerfeld integral. Here, J_n is the Bessel function of order n and (ρ, φ) are the cylindrical coordinates of the projection of the field point on the (x, y)-plane. Note that although (42)-(43) correspond to the case where the source is on the z-axis, they are easily generalized for arbitrary source locations by the substitutions

$$\rho \to \varrho = |\boldsymbol{\rho}-\boldsymbol{\rho}'|, \quad \varphi \to \phi = \arctan\frac{y-y'}{x-x'} \tag{44}$$

Finally, we note that the DGFs possess the reciprocity properties

$$\underline{\underline{\boldsymbol{G}}}^{EJ}(\boldsymbol{r}|\boldsymbol{r}') = \left[\underline{\underline{\boldsymbol{G}}}^{EJ}(\boldsymbol{r}'|\boldsymbol{r})\right]^T \tag{45}$$

$$\underline{\underline{\boldsymbol{G}}}^{HM}(\boldsymbol{r}|\boldsymbol{r}') = \left[\underline{\underline{\boldsymbol{G}}}^{HM}(\boldsymbol{r}'|\boldsymbol{r})\right]^T \tag{46}$$

$$\underline{\underline{\boldsymbol{G}}}^{EM}(\boldsymbol{r}|\boldsymbol{r}') = -\left[\underline{\underline{\boldsymbol{G}}}^{HJ}(\boldsymbol{r}'|\boldsymbol{r})\right]^T \tag{47}$$

which follow from (37)-(39) upon using (40)-(41).

V Derivation of Mixed Potential Representations

Consider first the case where only electric currents are present, i.e., $\boldsymbol{M} = \boldsymbol{0}$ in (11). It is then permissible to express the fields in terms of vector and scalar potentials through the equations

$$\mu_0 \underline{\underline{\boldsymbol{\mu}}} \cdot \boldsymbol{H} = \boldsymbol{\nabla} \times \boldsymbol{A}\,, \quad \boldsymbol{E} = -j\omega\boldsymbol{A} - \boldsymbol{\nabla}\Phi \tag{48}$$

The linearity of the problem allows us to write

$$\boldsymbol{A} = \mu_0 \left\langle \underline{\underline{\boldsymbol{G}}}^{A}; \boldsymbol{J} \right\rangle \tag{49}$$

where $\underline{\underline{\boldsymbol{G}}}^{A}(\boldsymbol{r}|\boldsymbol{r}')$ is the vector potential DGF. From (48) and (4) (with $\boldsymbol{M} = \boldsymbol{0}$) it follows that

$$\underline{\underline{\boldsymbol{\mu}}} \cdot \underline{\underline{\boldsymbol{G}}}^{HJ} = \boldsymbol{\nabla} \times \underline{\underline{\boldsymbol{G}}}^{A} \tag{50}$$

Since $\underline{\underline{\boldsymbol{G}}}^{HJ}$ has already been determined, we will use this relationship to obtain $\underline{\underline{\boldsymbol{G}}}^{A}$. The derivations are simplified in the spectrum domain, where the operator nabla becomes $\tilde{\boldsymbol{\nabla}} = -jk_\rho\hat{\boldsymbol{u}} + \hat{\boldsymbol{z}}d/dz$. Clearly, (50) does not uniquely specify $\underline{\underline{\boldsymbol{G}}}^{A}$, making different formulations possible [58]. Here, we postulate the form

$$\underline{\underline{\tilde{\boldsymbol{G}}}}^{A} = \underline{\underline{\boldsymbol{I}}}_t \tilde{G}^{A}_{vv} + \hat{\boldsymbol{z}}\hat{\boldsymbol{u}}\tilde{G}^{A}_{zu} + \hat{\boldsymbol{z}}\hat{\boldsymbol{z}}\tilde{G}^{A}_{zz} \tag{51}$$

which is consistent with the Sommerfeld's choice of potentials [99, p. 258] for a horizontal Hertzian dipole over a dielectric half-space. This is more evident when (51) is projected on the Cartesian coordinate system via (18) and put in the matrix form

$$\left[\tilde{G}^{A}\right] = \begin{bmatrix} \tilde{G}^{A}_{vv} & 0 & 0 \\ 0 & \tilde{G}^{A}_{vv} & 0 \\ \dfrac{k_x}{k_\rho}\tilde{G}^{A}_{zu} & \dfrac{k_y}{k_\rho}\tilde{G}^{A}_{zu} & \tilde{G}^{A}_{zz} \end{bmatrix} \tag{52}$$

which indicates that horizontal and vertical components of the vector potential are involved for a horizontal current source. To find the components of $\underline{\underline{\tilde{\boldsymbol{G}}}}^{A}(\boldsymbol{k}_\rho; z|z')$, we substitute (51) and (33) into the spectrum-domain counterpart of (50), which leads to the equations

$$j\omega\mu_0\tilde{G}^{A}_{vv} = V_i^h \tag{53}$$

$$j\omega\mu_0\tilde{G}^A_{zz} = \eta_0^2\frac{\mu_t}{\epsilon'_z}I^e_v \tag{54}$$

$$\frac{d}{dz}\tilde{G}^A_{vv} + jk_\rho\tilde{G}^A_{zu} = -\mu_t I^e_i \tag{55}$$

where $\eta_0 = \sqrt{\mu_0/\epsilon_0}$ is the intrinsic impedance of free-space. >From (55) and (53), upon using (26) and (22), we finally obtain

$$j\omega\mu_0\tilde{G}^A_{zu} = \frac{\omega\mu_0\mu_t}{k_\rho}\left(I^h_i - I^e_i\right) \tag{56}$$

The scalar potential may be found from the auxiliary condition

$$\boldsymbol{\nabla}\cdot(\mu_t^{-1}\mu_z^{-1}\underline{\underline{\boldsymbol{\mu}}}\cdot\boldsymbol{A}) = -j\omega\mu_0\epsilon_0\epsilon_t\Phi \tag{57}$$

which can be shown to be consistent with the vector potential obtained above. To arrive at the mixed-potential form of $\boldsymbol{E}$, we postulate the decomposition

$$\epsilon_t^{-1}\boldsymbol{\nabla}\cdot(\mu_t^{-1}\mu_z^{-1}\underline{\underline{\boldsymbol{\mu}}}\cdot\underline{\underline{\boldsymbol{G}}}^A) = -\boldsymbol{\nabla}'K^\Phi + C^\Phi\hat{\boldsymbol{z}} \tag{58}$$

where K^Φ is the scalar potential kernel and C^Φ is the *correction factor* which arises in general when both horizontal and vertical current components are present [39, 40, 58]. To find K^Φ and C^Φ, we substitute (51) in the spectrum-domain counterpart of (58), where $\tilde{\boldsymbol{\nabla}}' = jk_\rho\hat{\boldsymbol{u}} + \hat{\boldsymbol{z}}d/dz'$, which yields the equations

$$\tilde{K}^\Phi = \frac{1}{j\omega\mu_0\mu_z\epsilon_t}V^h_i + \frac{1}{k_\rho^2\epsilon_t}\frac{d}{dz}\left(I^h_i - I^e_i\right) \tag{59}$$

$$\tilde{C}^\Phi = \frac{1}{j\omega\epsilon_0\epsilon'_z\epsilon_t}\frac{d}{dz}I^e_v + \frac{d}{dz'}\tilde{K}^\Phi \tag{60}$$

Upon using (26)-(27) in the above, we finally arrive at

$$-\frac{\tilde{K}^\Phi}{j\omega\epsilon_0} = \frac{1}{k_\rho^2}\left(V^h_i - V^e_i\right) \tag{61}$$

$$-\frac{\tilde{C}^\Phi}{j\omega\epsilon_0} = \frac{j\omega\mu_0\mu'_t}{k_\rho^2}\left(V^h_v - V^e_v\right) \tag{62}$$

We next substitute (57) and (58) in the second equation of (48) and use the Gauss' theorem [80, p. 503] to obtain

$$\boldsymbol{E} = -j\omega\mu_0\langle\underline{\underline{\boldsymbol{G}}}^A;\boldsymbol{J}\rangle + \frac{1}{j\omega\epsilon_0}\boldsymbol{\nabla}\left(\langle K^\Phi,\boldsymbol{\nabla}'\cdot\boldsymbol{J}\rangle + \langle C^\Phi\hat{\boldsymbol{z}};\boldsymbol{J}\rangle\right) \tag{63}$$

The correction term in the above may be grouped with the vector potential term, resulting in the alternative mixed-potential representation

$$\boldsymbol{E} = -j\omega\mu_0\langle\underline{\underline{\boldsymbol{K}}}^A;\boldsymbol{J}\rangle + \frac{1}{j\omega\epsilon_0}\boldsymbol{\nabla}\langle K^\Phi,\boldsymbol{\nabla}'\cdot\boldsymbol{J}\rangle \tag{64}$$

where

$$\underline{\underline{\boldsymbol{K}}}^A = \underline{\underline{\boldsymbol{G}}}^A + \frac{1}{k_0^2}\boldsymbol{\nabla} C^\Phi \hat{\boldsymbol{z}} \tag{65}$$

is the modified vector potential kernel. The components of $\underline{\underline{\boldsymbol{K}}}^A$ are easily derived in the spectrum domain, where (65) becomes

$$\underline{\underline{\tilde{\boldsymbol{K}}}}^A = \underline{\underline{\tilde{\boldsymbol{G}}}}^A - \hat{\boldsymbol{u}}\hat{\boldsymbol{z}}\frac{jk_\rho}{k_0^2}\tilde{C}^\Phi + \hat{\boldsymbol{z}}\hat{\boldsymbol{z}}\frac{1}{k_0^2}\frac{d}{dz}\tilde{C}^\Phi \tag{66}$$

Upon substituting (62) and (51) in the above and using (27), we find

$$\underline{\underline{\tilde{\boldsymbol{K}}}}^A = \underline{\underline{\boldsymbol{I}}}_t \tilde{G}^A_{vv} + \hat{\boldsymbol{z}}\hat{\boldsymbol{u}}\tilde{G}^A_{zu} + \hat{\boldsymbol{u}}\hat{\boldsymbol{z}}\tilde{K}^A_{uz} + \hat{\boldsymbol{z}}\hat{\boldsymbol{z}}\tilde{K}^A_{zz} \tag{67}$$

where

$$j\omega\mu_0\tilde{K}^A_{uz} = \frac{\omega\mu_0\mu_t'}{k_\rho}\left(V_v^h - V_v^e\right) \tag{68}$$

$$j\omega\mu_0\tilde{K}^A_{zz} = \eta_0^2\frac{\mu_t}{\epsilon_z'}\left[\left(1 + \frac{\mu_t'\epsilon_z'}{\mu_t\epsilon_z}\right)I_v^e + \mu_t'\epsilon_z'\left(\frac{k_0}{k_\rho}\right)^2\left(I_v^h - I_v^e\right)\right] \tag{69}$$

We may also express $\underline{\underline{\tilde{\boldsymbol{K}}}}^A(\boldsymbol{k}_\rho; z|z')$ in the matrix form

$$\left[\tilde{K}^A\right] = \begin{bmatrix} \tilde{G}^A_{vv} & 0 & \frac{k_x}{k_\rho}\tilde{K}^A_{uz} \\ 0 & \tilde{G}^A_{vv} & \frac{k_y}{k_\rho}\tilde{K}^A_{uz} \\ \frac{k_x}{k_\rho}\tilde{G}^A_{zu} & \frac{k_y}{k_\rho}\tilde{G}^A_{zu} & \tilde{K}^A_{zz} \end{bmatrix} \tag{70}$$

Observe that $[\tilde{G}^A]$ and $[\tilde{K}^A]$ only differ in the third column, where one component has been modified and two new terms have appeared in the latter.

The spectral kernels $\underline{\underline{\tilde{\boldsymbol{K}}}}^A$ and $\tilde{K}^\Phi$ obtained above correspond to formulation C of Michalski and Zheng [58], which is in general preferable to formulations A and B, because its scalar potential kernel is a continuous function of both z and z' across the interfaces between dissimilar media (see Section VII). This property is desirable, because a discontinuous $\tilde{K}^\Phi$ would necessitate a contour integral to be added to the MPIE whenever the object penetrates an interface [58]. For planar conductors, formulation C reduces to the MPIE of Mosig and Gardiol [36].

The space-domain counterparts of the spectral kernels derived above can be expressed in terms of the Sommerfeld integrals via (42)-(43). In particular, we find

$$G^A_{xx}(\boldsymbol{\rho}; z|z') = G^A_{yy}(\boldsymbol{\rho}; z|z') = S_0\left\{\tilde{G}^A_{vv}(k_\rho; z|z')\right\} \tag{71}$$

$$G^A_{zz}(\boldsymbol{\rho}; z|z') = S_0\left\{\tilde{G}^A_{zz}(k_\rho; z|z')\right\} \tag{72}$$

$$G^A_{zx}(\boldsymbol{\rho}; z|z') = -j\cos\varphi\, S_1\left\{\tilde{G}^A_{zu}(k_\rho; z|z')\right\} \tag{73}$$

$$G^A_{zy}(\boldsymbol{\rho}; z|z') = -j\sin\varphi\, S_1\left\{\tilde{G}^A_{zu}(k_\rho; z|z')\right\} \tag{74}$$

$$K^{\Phi}(\boldsymbol{\rho};z|z') = S_0\left\{\tilde{K}^{\Phi}(k_\rho;z|z')\right\} \tag{75}$$

$$C^{\Phi}(\boldsymbol{\rho};z|z') = S_0\left\{\tilde{C}^{\Phi}(k_\rho;z|z')\right\} \tag{76}$$

Analogous expressions may be written for K^A_{xz}, K^A_{yz} and K^A_{zz}, but are omitted to conserve space. Recall that the substitutions (44) should be made before the above formulas are used in the MPIE. Also note that three distinct Sommerfeld integrals appear in $\underline{\underline{\boldsymbol{G}}}^A$, and four in $\underline{\underline{\boldsymbol{K}}}^A$.

It is easily shown, using (28), that $\underline{\underline{\boldsymbol{K}}}^A$ and K^{Φ} satisfy the reciprocity relations

$$\underline{\underline{\boldsymbol{K}}}^A(\boldsymbol{r}|\boldsymbol{r}') = \left[\underline{\underline{\boldsymbol{K}}}^A(\boldsymbol{r}'|\boldsymbol{r})\right]^T, \quad K^{\Phi}(\boldsymbol{r}|\boldsymbol{r}') = K^{\Phi}(\boldsymbol{r}'|\boldsymbol{r}) \tag{77}$$

which hold in general. A special case worth mentioning arises when the source and field points are confined to a homogeneous half-space. It then follows from the properties of the TLGFs (see Section VI) that $K^A_{xz} = -K^A_{zx}$ and $K^A_{yz} = -K^A_{zy}$. As a result, the contributions from the off-diagonal terms of $\underline{\underline{\boldsymbol{K}}}^A$ cancel each other in the MOM procedure for straight-wire segments located above or below a stratified half-space [39, 72].

Comparing the mixed-potential representations (63) and (64), we note that the latter closely resembles its homogeneous-space counterpart—the only difference being the dyadic character of the vector potential kernel. On the other hand, the form (63) comprises the correction term in the scalar potential, which does not appear in an unbounded homogeneous space. However, since this term introduces only minor complications in the numerical solution procedure [58, 67, 68], (63) may in fact be preferable to (64), because—as shown in Section VII—$\tilde{C}^{\Phi}$ converges faster as $k_\rho \to \infty$ than the terms introduced in the modified vector potential kernel (70).

In the case when only magnetic currents are present, the analysis is dual to that given above. The mixed-potential representations for $\boldsymbol{H}$ may be obtained from the above formulas by the following replacements of symbols: $\boldsymbol{E} \to \boldsymbol{H}$, $\boldsymbol{J} \to \boldsymbol{M}$, $\boldsymbol{A} \to \boldsymbol{F}$, $\Phi \to \Psi$, $\epsilon \to \mu$, $\mu \to \epsilon$, $V \to I$, $I \to V$, $v \to i$, $i \to v$, $e \to h$, and $h \to e$. Of course, this application of duality does not save any computation time; it merely allows us to conserve space here and to avoid unnecessary derivations.

When both electric and magnetic currents are present, we use superposition and, in view of (3)-(4), arrive at the mixed-potential forms (5)-(6) when (63) and its dual are used, or at (7)-(8) when (64) and its dual are employed.

VI Derivation of Transmission-Line Green's Functions

The theory developed so far is for an unspecified stratification, since no assumption has been made regarding the z-dependence of the media parameters. We now specialize it to the case of a multilayered medium with piecewise-constant parameters. The parameters pertaining to layer n, with boundaries at z_n and z_{n+1}, are distinguished by a subscript n. The transmission line analog of the layered medium consists of a cascade connection of uniform transmission line sections, where section n, with terminals at z_n and z_{n+1}, has propagation constant k^p_{zn} and characteristic impedance Z^p_n. To find the TLGFs, we excite the transmission line network by unit-strength voltage and current sources at z' and compute the voltage and current at z. Without loss of generality we assume that z' and z are within

sections n and m, respectively. Hence, the primed media parameters assume the values pertaining to layer n, while the unprimed ones are those of layer m.

The source section is illustrated in Fig. 5, where $\overleftarrow{\Gamma}_n^p$ and $\vec{\Gamma}_n^p$ are the voltage reflection coefficients looking to the left and right, respectively, out of the terminals of section n. These coefficients, which are referred to z_n and z_{n+1}, respectively, may be computed from the recursive relations

$$\overleftarrow{\Gamma}_{n+1}^p = \frac{\Gamma_{n,n+1}^p + \overleftarrow{\Gamma}_n^p\, t_n^p}{1 + \Gamma_{n,n+1}^p\, \overleftarrow{\Gamma}_n^p\, t_n^p}, \quad \vec{\Gamma}_{n-1}^p = \frac{\Gamma_{n,n-1}^p + \vec{\Gamma}_n^p\, t_n^p}{1 + \Gamma_{n,n-1}^p\, \vec{\Gamma}_n^p\, t_n^p} \tag{78}$$

where $t_n^p = e^{-j2k_{zn}^p d_n}$ with $d_n = z_{n+1} - z_n$, and where

$$\Gamma_{ij}^p = \frac{Z_i^p - Z_j^p}{Z_i^p + Z_j^p} \tag{79}$$

These formulas follow from the source-free transmission-line equations (20) and the continuity of the voltages and currents at the line junctions. One computes the left-looking reflection coefficients working from the left end to the right end of the transmission line network. The starting value, $\overleftarrow{\Gamma}_1^p$, is easily found, for if the first layer is of infinite extent, then it is reflectionless and $\overleftarrow{\Gamma}_1^p = 0$. If, on the other hand, the first layer is backed by a conducting ground plane with surface impedance Z_s, then

$$\overleftarrow{\Gamma}_1^p = \frac{Z_s - Z_1^p}{Z_s + Z_1^p} \tag{80}$$

which becomes -1 if the ground plane is made of a PEC. Similar remarks apply to the right-looking reflection coefficients, which are computed working from the right end to the left end of the network.

Consider first the case $m = n$, when z lies within the source section. The TLGF V_i^p is then readily determined from (26) as

$$V_i^p(z|z') = Z_n^p \frac{e^{-jk_{zn}^p|z-z'|}}{2D_n^p} \left[1 + \overleftarrow{\Gamma}_n^p\, e^{-j2k_{zn}^p(z_< - z_n)}\right] \left[1 + \vec{\Gamma}_n^p\, e^{-j2k_{zn}^p(z_{n+1} - z_>)}\right] \tag{81}$$

where $z_< = \min(z, z')$, $z_> = \max(z, z')$, and where $D_n^p = 1 - \overleftarrow{\Gamma}_n^p \vec{\Gamma}_n^p\, t_n^p$. A more revealing form of (81) is

$$V_i^p(z|z') = \frac{Z_n^p}{2} \left[e^{-jk_{zn}^p|z-z'|} + \frac{1}{D_n^p} \sum_{s=1}^{4} R_{ns}^p e^{-jk_{zn}^p y_{ns}}\right] \tag{82}$$

where

$$\begin{aligned} y_{n1} &= 2z_{n+1} - (z + z'), \quad y_{n2} = (z + z') - 2z_n, \\ y_{n3} &= 2d_n + (z - z'), \quad y_{n4} = 2d_n - (z - z') \end{aligned} \tag{83}$$

and

$$R_{n1}^p = \vec{\Gamma}_n^p, \quad R_{n2}^p = \overleftarrow{\Gamma}_n^p, \quad R_{n3}^p = R_{n4}^p = \overleftarrow{\Gamma}_n^p \vec{\Gamma}_n^p \tag{84}$$

The first term in (82) represents the direct ray between the source and the field point, while the second term represents the rays that undergo partial reflections at the upper and lower slab boundaries before reaching the observation point.

The remaining TLGFs may readily be derived from (81) or (82) upon using (26)-(28). For example, one may obtain I_i^p from V_i^p via the first equation of (26), from which V_v^p follows via the third equation of (28). The result is

$$V_v^p(z|z') = \pm\frac{e^{-jk_{zn}^p|z-z'|}}{2D_n^p}\left[1\mp\overleftarrow{\Gamma}_n^p\, e^{-j2k_{zn}^p(z_<-z_n)}\right]\left[1\pm\vec{\Gamma}_n^p\, e^{-j2k_{zn}^p(z_{n+1}-z_>)}\right] \tag{85}$$

with the alternative form

$$V_v^p(z|z') = \frac{1}{2}\left[\pm e^{-jk_{zn}^p|z-z'|} - \frac{1}{D_n^p}\sum_{s=1}^{4}(-1)^s R_{ns}^p e^{-jk_{zn}^p\gamma_{ns}}\right] \tag{86}$$

where the upper and lower signs pertain to $z > z'$ and $z < z'$, respectively. To conserve space, we do not list the expressions for I_v^p and I_i^p which—as is evident from (26)-(27)—are dual to those for V_i^p and V_v^p, respectively, and may be obtained from the latter by replacing the impedances by admittances (which has also the effect of changing the signs of the reflection coefficients). We note from (61)-(62) that the discontinuous terms appearing in V_v^p and I_i^p cancel out when the TE and TM transmission-line Green's functions are subtracted to form $\tilde{K}^\Phi$ and $\tilde{C}^\Phi$.

Consider next the case $m < n$, i.e., z is outside the source section and $z < z'$. Given the voltage $V^p(z_n)$ across the left terminals of section n, the voltage $V^p(z)$ and current $I^p(z)$ at any point z in section m can be found from the homogeneous form of the transmission-line equations (20) as [100]

$$\left\{\begin{array}{c} V^p(z) \\ I^p(z) \end{array}\right\} = V^p(z_n)\frac{\prod_{k=m+1}^{n-1}\overleftarrow{T}_k^p}{1+\overleftarrow{\Gamma}_m^p t_m^p}\left\{\begin{array}{c} \overleftarrow{\tau}_m^p(z) \\ \overleftarrow{\mathcal{Y}}_m^p(z) \end{array}\right\} e^{-jk_{zm}^p(z_{m+1}-z)} \tag{87}$$

where

$$\overleftarrow{T}_k^p \equiv \frac{V^p(z_k)}{V^p(z_{k+1})} = \frac{(1+\overleftarrow{\Gamma}_k^p)\theta_k^p}{1+\overleftarrow{\Gamma}_k^p t_k^p} \tag{88}$$

with $\theta_k^p = e^{-jk_{zk}^p d_k}$, and where

$$\overleftarrow{\tau}_m^p(z) = \left[1+\overleftarrow{\Gamma}_m^p\, e^{-j2k_{zm}^p(z-z_m)}\right] \tag{89}$$

$$\overleftarrow{\mathcal{Y}}_m^p(z) = -Y_m^p\left[1-\overleftarrow{\Gamma}_m^p\, e^{-j2k_{zm}^p(z-z_m)}\right] \tag{90}$$

It is understood that the product in (87) is equal to one if the lower limit exceeds the upper limit. Note that (87) is applicable irrespective of the source type. Hence, if section n is excited by a unit-strength current source at z', then $V^p(z_n) = V_i^p(z_n|z')$, and $V^p(z)$ and $I^p(z)$ represent $V_i^p(z|z')$ and $I_i^p(z|z')$, respectively. If, on the other hand, section n is excited by a unit-strength voltage source at z', then $V^p(z_n) = V_v^p(z_n|z')$, and $V^p(z)$ and $I^p(z)$ represent $V_v^p(z|z')$ and $I_v^p(z|z')$, respectively.

Analogous formulas may be developed for the case $m > n$, i.e., when z is outside the source section and $z > z'$. However, this is hardly necessary because the reciprocity theorems (28) allow one to interchange the source and field point locations. For example, $V_v^p(z|z')$ may be computed as $-I_i^p(z'|z)$. This application of reciprocity also results in a shorter and more efficient computer code.

The formulas presented in this section easily specialize to the case where the source or observation layer is of infinite thickness (i.e., it forms a half-space) and thus either the left- or right-looking reflection coefficient becomes zero—one simply omits the terms multiplying the vanishing reflection coefficients. It is also worth noting that all exponentials in the above are non-growing, which reduces the danger of overflows and underflows in numerical computations.

VII Discussion of Sommerfeld Integrals

The computation of the Sommerfeld integrals (43) is a difficult task because of the in general oscillatory and divergent behavior of the integrands and the occurrence of singularities near the integration path in the complex k_ρ-plane [42, 43]. Since these integrals must be repeatedly evaluated in filling of the MOM matrix, their efficient computation is of paramount importance and has been the subject of much research. Nevertheless, it is fair to say that a completely satisfactory solution to this problem is still lacking, especially in the case of arbitrarily shaped objects extending over more than one layer of the multilayered medium. A detailed treatment of the Sommerfeld integration being outside the scope of this article, here we only touch upon a few aspects of the procedure—especially those related to the transmission-line formalism and the MPIE.

The integrand singularities, which occur in complex-conjugate pairs in the second and fourth quadrants of the k_ρ-plane, consist of poles and branch points [101, p. 111]. In the lossless case some of these singularities appear on the real axis and the integration path in (43) must be indented into the first quadrant to avoid them. The branch points only occur for vertically unbounded media, i.e., when the top and/or the bottom layer is a half-space. In this case the integration path must be on the proper sheet of the Riemann surface associated with the longitudinal propagation wavenumbers (21) of the half-spaces. The poles are associated with the TM and TE guided waves and are found as roots of the resonant denominator D_n^p in any finite-thickness layer, or as roots of the denominator of one of the reflection coefficients (78) looking into the layered medium from a half-space. The number of poles is in general infinite, but only a finite number of them appear on the proper sheet in the case of vertically unbounded media. Observe that only TE poles occur in $\tilde{G}_{xx}^A$ and $\tilde{G}_{yy}^A$, only TM poles in $\tilde{G}_{zz}^A$, while both sets are involved in $\tilde{G}_{zx}^A$, $\tilde{G}_{zy}^A$, $\tilde{K}^\Phi$, and $\tilde{C}^\Phi$. Various integration paths in the k_ρ-plane have been employed [36, 59, 102, 103], but the real-axis path, indented into the first quadrant to avoid the branch-point and pole singularities [104], has proven to be most convenient for multilayered media, because it obviates the need to locate the poles. When $\varrho > 0$, the integral over the real axis tail of the path is computed as a sum of an alternating series of integrals between zeros of the Bessel function. To speed up the convergence, series acceleration techniques—such as the method of averages [36, 43, 105] or the continued fraction expansion [106]—are applied.

Before attempting to compute the Sommerfeld integrals, it is important to understand the asymptotic (quasi-static) behavior of their integrands as $k_\rho \to \infty$. This knowledge is needed, for example, in the method of averages, or to extract the quasi-static parts from the spectral kernels—both as a measure to accelerate the Sommerfeld integrals and to isolate the singular parts of the kernels [66]. Since all kernels have been expressed in terms of the TLGFs, much insight is gained by investigating the asymptotic behavior of the latter. As is evident from (82), (86) and their dual equations, these functions decay exponentially unless $z = z'$, which represents the worst-case situation. We will therefore focus attention on the case where z lies within the source layer. The quasi-static forms of V_i^p and V_v^p are readily found from (82) and (86) by expanding D_n^p in a geometric series and replacing the reflection coefficients by their asymptotic values. Each term of the series then represents a quasi-static image of the source. Keeping only the direct components and two dominant image terms, we find that as $k_\rho \to \infty$

$$V_i^p \sim \frac{Z_n^{p\infty}}{2}\left[e^{-jk_{zn}^p|z-z'|} + \chi_{n+1,n}^p\, e^{-jk_{zn}^p \gamma_{n1}} + \chi_{n-1,n}^p\, e^{-jk_{zn}^p \gamma_{n2}}\right] \tag{91}$$

$$V_v^p \sim \frac{1}{2}\left[\pm e^{-jk_{zn}^p|z-z'|} + \chi_{n+1,n}^p\, e^{-jk_{zn}^p \gamma_{n1}} - \chi_{n-1,n}^p\, e^{-jk_{zn}^p \gamma_{n2}}\right] \tag{92}$$

where

$$Z_n^{e\infty} = \frac{k_\rho}{j\omega\epsilon_0\kappa_n^e}, \quad Z_n^{h\infty} = \frac{j\omega\mu_0\kappa_n^h}{k_\rho} \tag{93}$$

with $\kappa_n^e = \sqrt{\epsilon_{tn}\epsilon_{zn}}$, $\kappa_n^h = \sqrt{\mu_{tn}\mu_{zn}}$, and where

$$\chi_{ij}^e = -\frac{\kappa_i^e - \kappa_j^e}{\kappa_i^e + \kappa_j^e}, \quad \chi_{ij}^h = \frac{\kappa_i^h - \kappa_j^h}{\kappa_i^h + \kappa_j^h}, \tag{94}$$

The quasi-static behavior of I_v^p and I_i^p may be found from (91) and (92) by using duality, as explained in the paragraph following (86). The worst-case asymptotic behavior of the TLGFs is now evident and is summarized for easy reference in Table II. By referring to this table, one can easily ascertain the asymptotic behavior of the spectral kernels and determine which ones would benefit most from the quasi-static part extraction. For example, we find that all components of $\underline{\underline{\tilde{G}}}^A$ and $\tilde{K}^\Phi$ are $\mathcal{O}(k_\rho^{-1})$, while $\tilde{C}^\Phi$ is $\mathcal{O}(k_\rho^{-2})$.

The asymptotic extraction is only feasible if the quasi-static part can be Fourier-inverted in closed form. Fortunately, in many cases this may be accomplished by means of the formula

$$S_0\left\{\frac{e^{-jk_{zn}^p|z|}}{2jk_{zn}^p}\right\} = \frac{e^{-jk_{tn}r_n^p}}{4\pi\nu_n^p r_n^p}, \quad r_n^p = \sqrt{\rho^2/\nu_n^p + z^2} \tag{95}$$

which is the Sommerfeld identity [101, p. 66] extended to a uniaxial medium. Applying this procedure to G_{xx}^A, we obtain the asymptotic form

$$\tilde{G}_{xx}^{A\infty} = \frac{\mu_{tn}}{2jk_{zn}^h}\left[e^{-jk_{zn}^h|z-z'|} + \chi_{n+1,n}^h\, e^{-jk_{zn}^h \gamma_{n1}} + \chi_{n-1,n}^h\, e^{-jk_{zn}^h \gamma_{n2}}\right] \tag{96}$$

which is clearly amenable to (95) and leads to

$$G_{xx}^{A\infty} = \frac{\mu_{zn}}{4\pi}\left[\frac{e^{-jk_{tn}r_{n0}^h}}{r_{n0}^h} + \chi_{n+1,n}^h\,\frac{e^{-jk_{tn}r_{n1}^h}}{r_{n1}^h} + \chi_{n-1,n}^h\,\frac{e^{-jk_{tn}r_{n2}^h}}{r_{n2}^h}\right] \tag{97}$$

where

$$r_{n0}^p = \sqrt{\rho^2/\nu_n^p + (z-z')^2}\,, \quad r_{ni}^p = \sqrt{\rho^2/\nu_n^p + \gamma_{ni}^2}\,, \quad i = 1,2 \tag{98}$$

Similarly, for G_{zz}^A and K^Φ, we obtain

$$\tilde{G}_{zz}^{A\infty} = \frac{\mu_{tn}\nu_n^e}{2jk_{zn}^e}\left[e^{-jk_{zn}^e|z-z'|} - \chi_{n+1,n}^e\, e^{-jk_{zn}^e\gamma_{n1}} - \chi_{n-1,n}^e\, e^{-jk_{zn}^e\gamma_{n2}}\right] \tag{99}$$

$$G_{zz}^{A\infty} = \frac{\mu_{tn}}{4\pi}\left[\frac{e^{-jk_{tn}r_{n0}^e}}{r_{n0}^e} - \chi_{n+1,n}^e\,\frac{e^{-jk_{tn}r_{n1}^e}}{r_{n1}^e} - \chi_{n-1,n}^e\,\frac{e^{-jk_{tn}r_{n2}^e}}{r_{n2}^e}\right] \tag{100}$$

and

$$\tilde{K}^{\Phi\infty} = \frac{1}{2jk_{zn}^e\epsilon_{zn}}\left[e^{-jk_{zn}^e|z-z'|} + \chi_{n+1,n}^e\, e^{-jk_{zn}^e\gamma_{n1}} + \chi_{n-1,n}^e\, e^{-jk_{zn}^e\gamma_{n2}}\right] \tag{101}$$

$$K^{\Phi\infty} = \frac{1}{4\pi\epsilon_{tn}}\left[\frac{e^{-jk_{tn}r_{n0}^e}}{r_{n0}^e} + \chi_{n+1,n}^e\,\frac{e^{-jk_{tn}r_{n1}^e}}{r_{n1}^e} + \chi_{n-1,n}^e\,\frac{e^{-jk_{tn}r_{n2}^e}}{r_{n2}^e}\right] \tag{102}$$

The quasi-static parts that arise in the case of G_{zx}^A, $G_{z\mathcal{Y}}^A$ and C^Φ are not invertible in closed form. However, this undesirable situation is somewhat mitigated by the fact that there is a cancellation of the direct components in the spectral kernels involved.

An important benefit of the quasi-static form extraction is the isolation of the singular whole-space part of the kernel, which may be handled just as the free-space potential Green's function in the MOM procedure. Furthermore, when z and z' are on an interface, one of the image terms also becomes singular upon inversion, and must be handled accordingly. In fact, only the singular (or near-singular) image term is essential, and the other may be omitted. It should be noted that when the quasi-static forms given above are subtracted from the respective spectral kernels, the direct terms cancel exactly for G_{xx}^A and G_{zz}^A, but only asymptotically for K^Φ. Finally, one potentially detrimental effect of this extraction procedure should be mentioned. Namely, in the case of a layer of finite thickness, the quasi-static terms introduce a new pair of branch-points in the k_ρ-plane, thus making the modified integrand more rapidly varying in the intermediate k_ρ-range on the integration path [107].

Even with the state-of-the-art techniques, the Sommerfeld integrals may take a significant part of the overall computational effort involved in the solution of the MPIE. One attractive remedy is to precompute these integrals on a grid of points in the solution domain and to use table look-up and interpolation techniques. For arbitrarily shaped objects, three-dimensional interpolation in ϱ, z, and z' is required [2]. Alternatively, one may split the kernels into parts depending on $(\varrho, z-z')$ and $(\varrho, z+z')$, and compute them separately using two-dimensional interpolations [102]. Only one-dimensional interpolation in ϱ is needed for strictly planar microstrip structures, which leads to a particularly efficient solution procedure [43, 105].

Since one should avoid interpolating across points where the function or its derivative is discontinuous, it is important to ascertain the behavior of the MPIE kernels at the layer interfaces. Fortunately, this behavior is evident from (71)-(76), because the Sommerfeld integrals involved are continuous functions of z and z'. For example, it is clear that G_{zz}^A undergoes a 'jump' as the source point crosses an interface—unless the contiguous layers have the same ϵ_z, and it also jumps when the observation point crosses an interface—unless the contiguous layers have the same μ_t. Furthermore, G_{xx}^A and K^Φ are always continuous

at the interfaces, but have discontinuous derivatives there with respect to z and z'. Consequently, a safe procedure is to place grid points on both sides of each interface, and to never interpolate across it.

Another approach that came into prominence recently is the discrete complex image method (DCIM) [50, 107–113]. The basic idea of the DCIM is to extract from the spectral kernel its quasi-static part—exactly as described above, and its guided-wave terms, and to approximate the remainder function by a sum of complex exponentials, using an established systems identification procedure [114]. The Sommerfeld integrals are then evaluated in closed form via (95). Since this method obviates numerical integration, it affords at least an order-of-magnitude speed-up in the MOM matrix fill time [115]. However, the DCIM has no built-in convergence measures and its accuracy can only be ascertained *a posteriori* by checking the results against those obtained by Sommerfeld integration. Furthermore, the application of the DCIM in multilayered media is currently impeded by the lack of reliable automated procedures for the extraction of the guided-wave poles.

VIII Extension to Shielded Environments

Although the formulation presented so far can easily accommodate horizontal perfectly conducting or impedance ground planes, the underlying assumption has been that the layered medium is of infinite lateral extent. We now extend this theory to the practically important case of a layered medium enclosed by a rectangular shield with PEC walls. The cross-sectional dimensions of the shield are $a \times b$, as illustrated in Fig. 6. Note that the shield forms a rectangular waveguide along the z-axis [116], or a rectangular cavity—if it is sandwiched between horizontal ground planes [117]. The approach we present here is based on the image theory [79, p. 103], which makes it possible to represent the effect of the side walls by a set of image sources radiating in a laterally unbounded medium [118].

To begin with, consider a point charge q located at (x', y', z') inside the rectangular shield and its three images located at $(-x', y', z')$, $(x', -y', z')$, and $(-x', -y', z')$, as illustrated in Fig. 6. Note that the polarities (signs) of these images are consistent with the boundary conditions at two intersecting PEC ground planes defined by $x = 0$ and $y = 0$. The so-constructed four-source set (the original source plus the three images) forms the *basic image set* (BIS). Note that the BIS is located within the $2a \times 2b$ *reference cell* centered at $(x, y) = (0, 0)$. Similar image sets may be constructed for x-, y-, and z-oriented current elements. The polarities of the images for different sources are conveniently described by two sign coefficients, s_x and s_y, where $s_\nu = +1$ if the polarity of the image in the $\nu = 0$ PEC wall is the same as that of the original source, and $s_\nu = -1$ if the imaged source undergoes a sign reversal. The values of s_x and s_y for electric sources are listed in Table III. For magnetic sources, all signs should be reversed.

To maintain the correct boundary conditions at the four side walls, the BIS of the reference cell must be imaged in the $x = a$ and $y = b$ PEC planes, and the new image sets must again be imaged in the $x = 0$ and $y = 0$ planes, etc. As a result, a doubly periodic lattice of BISs is obtained, with periods $2a$ and $2b$ along the x- and y-axes, respectively. Since these sources are now embedded in a transversely unbounded medium, they may be analyzed within the framework of the theory developed in the previous sections. Hence, if

$G(x-x',z-z';z|z')$ is a scalar potential kernel or a scalar component of a dyadic kernel (or Green's function) in the *laterally open medium*, we find that the corresponding kernel $\mathcal{G}(\boldsymbol{r}|\boldsymbol{r}')$ in the *laterally shielded environment* is given by

$$\begin{aligned}\mathcal{G}(\boldsymbol{r}|\boldsymbol{r}') = \sum_{m=-\infty}^{+\infty}\sum_{n=-\infty}^{+\infty} \{&G(x-x'+2ma, y-y'+2nb; z|z') \\ &+ s_x G(x+x'-2ma, y-y'+2nb; z|z') \\ &+ s_y G(x-x'+2ma, y+y'-2nb; z|z') \\ &+ s_x s_y G(x+x'-2ma, y+y'-2nb; z|z')\}\end{aligned} \tag{103}$$

The sign coefficients s_x and s_y in the above depend on the type of the kernel or Green's function considered. For example, if G represents G^A_{zx}, which is the z-component of the vector potential Green's function due to an x-directed current element, we find from Table III that $s_x = +1$ and $s_y = -1$. For the scalar potential and correction kernels K^Φ and C^Φ, the sign coefficients are those associated with q.

The spatial sum (103) may be transformed by the Poisson's formula [119, p. 47]

$$\sum_{m=-\infty}^{+\infty}\sum_{n=-\infty}^{+\infty} f(x-2ma, y-2nb) = \frac{1}{4ab}\sum_{m=-\infty}^{+\infty}\sum_{n=-\infty}^{+\infty} \tilde{f}(k_{xm}, k_{yn}) e^{-j(k_{xm}x+k_{yn}y)} \tag{104}$$

where $k_{xm} = m\pi/a$, $k_{yn} = n\pi/b$ into the spectral sum [120]

$$\begin{aligned}\mathcal{G}(\boldsymbol{r}|\boldsymbol{r}') = \frac{1}{4ab}\sum_{m=-\infty}^{+\infty}\sum_{n=-\infty}^{+\infty} &\tilde{G}(k_{xm}, k_{yn}; z|z') e^{-j(k_{xm}x+k_{yn}y)} \\ &\times \left(e^{jk_{xm}x'} + s_x e^{-jk_{xm}x'}\right)\left(e^{jk_{yn}y'} + s_y e^{-jk_{yn}y'}\right)\end{aligned} \tag{105}$$

Furthermore, the series in the above may be folded, with the result

$$\begin{aligned}\mathcal{G}(\boldsymbol{r}|\boldsymbol{r}') = \frac{1}{ab}\sum_{m=0}^{\infty}\sum_{n=0}^{\infty} &\varepsilon_m \varepsilon_n \tilde{G}(k_{xm}, k_{yn}; z|z') \\ &\times T_x(k_{xm}x) S_x(k_{xm}x') T_y(k_{yn}y) S_y(k_{yn}y')\end{aligned} \tag{106}$$

where $\varepsilon_n = 1$ for $n = 0$ and $\varepsilon_n = 2$ for $n > 0$, and where

$$S_\nu(\xi) = \begin{cases} \cos\xi, & s_\nu = +1 \\ j\sin\xi, & s_\nu = -1 \end{cases} \tag{107}$$

$$T_\nu(\xi) = \begin{cases} \cos\xi, & s_\nu \cdot c_\nu = +1 \\ -j\sin\xi, & s_\nu \cdot c_\nu = -1 \end{cases} \tag{108}$$

We have introduced in the above the sign coefficients c_x and c_y, defined as follows: $c_\nu = +1$ (-1) if $\tilde{G}$ is an even (odd) function of k_ν. For example, if G represents G^A_{zx}, the inspection of (52) and (56) indicates that $c_x = -1$ and $c_y = +1$. When the reference cell in Fig. 6 is centered at an arbitrary point (x_0, y_0), rather than at $(0,0)$, the above formulas must be modified by the substitutions $(x,y) \to (x-x_0, y-y_0)$ and $(x',y') \to (x'-x_0, y'-y_0)$.

The double series in (106) is slowly convergent, especially when $z = z'$—which is often the case in the analysis of planar microstrip structures, and must in practice be accelerated. This may be accomplished by subtracting from $\tilde{G}$ its quasi-static form $\tilde{G}^{\infty}$ (see Section VII), which converts (106) into a rapidly converging series, because $\tilde{G}$ and $\tilde{G}^{\infty}$ have the same asymptotic behavior. The double series of the subtracted quasi-static terms is then added back in its spatial form (103). Since the latter is comprised of the direct and quasi-static image terms, it is amenable to the well-established acceleration methods [68, 121–124]. These techniques employ mixed-domain representations involving both a space-domain and a spectrum-domain series and have an arbitrary parameter which distributes the computational burden between the two domains. In a simpler approach [125, 126], one of the asymptotic series is left in the space domain and the other is transformed via a one-dimensional Poisson's formula, leading to a rapidly-convergent series of modified Bessel functions of the second kind. As explained in the previous section, the asymptotic subtraction procedure is only applicable to kernels with quasi-static terms which may be inverted via (95).

When kernels of the form (106) are used in the MPIEs (9)-(10), the integrals may be introduced inside the summations and—for simple enough basis and testing functions—evaluated analytically. This is easily done when z and z' are fixed—a common situation for planar microstrip structures, but the integrations are tedious in the general case, because of the rather complicated dependence of the TLGFs on z and z', as discussed in Section VI. Note that this method may be classified as a three-dimensional SDA for laterally shielded environments.

IX Derivation of Far-Zone Field

Let $(\boldsymbol{J}_s, \boldsymbol{M}_s)$ be known surface currents on a surface S embedded in a layered medium which is not shielded from above. Assume that the upper half-space is filled with air, which is the most common situation in practice. Let z_0 be a point on the z-axis such that the layered medium and the surface S are confined to the region $z \leq z_0$, as illustrated in Fig. 7. Our goal is to derive leading-order asymptotic expressions for the fields radiated by $(\boldsymbol{J}_s, \boldsymbol{M}_s)$, valid when the field point is far from S in the half-space region $z \geq z_0$.

It should be clear from (32)-(35) and the TLGFs given in Section VI that in the region of interest the spectral DGFs may be expressed as

$$\underline{\underline{\tilde{\boldsymbol{G}}}}^{PQ}(\boldsymbol{k}_\rho; z|z') = \underline{\underline{\tilde{\boldsymbol{G}}}}^{PQ}(\boldsymbol{k}_\rho; z_0|z')\, e^{-jk_z(z-z_0)}, \quad z \geq z_0 \tag{109}$$

where $k_z = \sqrt{k_0^2 - k_\rho^2}$. In view of (40)-(41), the space-domain counterpart of (109) may be written as

$$\underline{\underline{\boldsymbol{G}}}^{PQ}(\boldsymbol{r}|\boldsymbol{r}') = \frac{1}{(2\pi)^2} \int_{-\infty}^{+\infty}\int_{-\infty}^{+\infty} 2jk_z\, \underline{\underline{\tilde{\boldsymbol{G}}}}^{PQ}(\boldsymbol{k}_\rho; z_0|z') \left\{ \frac{e^{-j\boldsymbol{k}\cdot(\boldsymbol{r}-\boldsymbol{r}_0')}}{2jk_z} \right\} dk_x dk_y \tag{110}$$

where $\boldsymbol{k} = \boldsymbol{k}_\rho + \hat{\boldsymbol{z}} k_z$, $\boldsymbol{r}_0' = \boldsymbol{\rho}' + \hat{\boldsymbol{z}} z_0$. The integrand in (110) has been factorized into a slowly-varying part and a rapidly varying part, where the latter (enclosed in curly braces) can be integrated in closed form via the Sommerfeld identity (95). As $r \to \infty$ along a ray specified

by the spherical angles (ϑ, φ), most of the contribution to the integral comes from the vicinity of the stationary-phase point at $k_{xo} = k_0 x/r$, $k_{yo} = k_0 y/r$ [127]. We may therefore replace the slowly-varying part of the integrand with its value at the stationary-phase point and evaluate the integral in closed form. As a result, upon invoking the usual far-zone approximations [79, p. 132], we obtain

$$\underline{\underline{\boldsymbol{G}}}^{PQ}(\boldsymbol{r}|\boldsymbol{r}') \sim -\frac{e^{-jk_0 r}}{2\pi jr}\, e^{jk_{zo}z_0}\, k_{zo}\, \underline{\underline{\tilde{\boldsymbol{G}}}}^{PQ}(\boldsymbol{k}_{\rho o}; z_0|z')\, e^{j\boldsymbol{k}_{\rho o}\cdot\boldsymbol{\rho}'}, \quad r \to \infty \tag{111}$$

where $k_{zo} = k_0 \cos\vartheta$ and $\boldsymbol{k}_{\rho o} = \hat{\boldsymbol{\rho}} k_{\rho o}$ with $k_{\rho o} = k_0 \sin\vartheta$. Here $0 \le \vartheta < \pi/2$ and

$$\boldsymbol{k}_{\rho o} \cdot \boldsymbol{\rho}' = k_0 \sin\vartheta\, (x' \cos\varphi + y' \sin\varphi) \tag{112}$$

Note that at the stationary-phase point $(\hat{\boldsymbol{u}}, \hat{\boldsymbol{v}}) = (\hat{\boldsymbol{\rho}}, \hat{\boldsymbol{\varphi}})$, where the directions of the unit vectors $\hat{\boldsymbol{\rho}}$ and $\hat{\boldsymbol{\varphi}} = \hat{\boldsymbol{z}} \times \hat{\boldsymbol{\rho}}$ are fixed by the observation angle φ. Hence, upon substituting (111) together with (32) and (34) into (3) and using (26)-(27), we find that the far-zone electric field components may be expressed as [128]

$$E_{\vartheta,\varphi} \sim \frac{e^{-jk_0 r}}{2\pi jr}\, e^{jk_{zo}z_0}\, k_0 \left(\langle \boldsymbol{f}^{EJ}_{\vartheta,\varphi}\, e^{j\boldsymbol{k}_{\rho o}\cdot\boldsymbol{\rho}'}; \boldsymbol{J}_s \rangle + \eta_0 \langle \boldsymbol{f}^{EM}_{\vartheta,\varphi}\, e^{j\boldsymbol{k}_{\rho o}\cdot\boldsymbol{\rho}'}; \boldsymbol{M}_s \rangle \right), \quad r \to \infty \tag{113}$$

where

$$\boldsymbol{f}^{EJ}_{\vartheta} = V^e_i(z_0|z')\hat{\boldsymbol{\rho}} - \frac{\eta_0^2}{\epsilon'_z} \sin\vartheta \cos\vartheta\, I^e_v(z_0|z')\hat{\boldsymbol{z}} \tag{114}$$

$$\boldsymbol{f}^{EJ}_{\varphi} = \cos\vartheta\, V^h_i(z_0|z')\hat{\boldsymbol{\varphi}} \tag{115}$$

$$\boldsymbol{f}^{EM}_{\vartheta} = \cos\vartheta\, I^e_v(z_0|z')\hat{\boldsymbol{\varphi}} \tag{116}$$

$$\boldsymbol{f}^{EM}_{\varphi} = -I^h_v(z_0|z')\hat{\boldsymbol{\rho}} + \frac{1}{\eta_0^2 \mu'_z} \sin\vartheta \cos\vartheta\, V^h_i(z_0|z')\hat{\boldsymbol{z}} \tag{117}$$

It is understood in the above that the TLGFs are evaluated with $k_\rho = k_{\rho o}$. Once the far-zone electric field is found, the corresponding magnetic field readily follows [79, p. 133].

The simple far-zone approximations derived here are only valid when the integrand in (110) does not have any singularities near the stationary-phase point. Also, they do not include contributions from the guided-wave poles, which may be important when the field point is near the air-dielectric interface [129].

X Derivation of Plane-Wave Impressed Field

Consider a plane wave with the electric field amplitude E_0 propagating in free space. The direction of arrival of this wave is specified by the angles (ϑ_i, φ_i) and its polarization by ζ_i, as illustrated in Fig. 8. Projected on the cylindrical coordinate system, the electric field is given as

$$\boldsymbol{E}^i_0 = E_0 \left[(\hat{\boldsymbol{\rho}}_i \cos\vartheta_i + \hat{\boldsymbol{z}} \sin\vartheta_i) \cos\zeta_i + \hat{\boldsymbol{\varphi}}_i \sin\zeta_i \right] e^{jk_{zi}(z-z_0)}\, e^{-j\boldsymbol{k}_{\rho i}\cdot\boldsymbol{\rho}} \tag{118}$$

where z_0 is an arbitrarily chosen phase reference point on the z-axis, and where $k_{zi} = k_0 \cos\vartheta_i$ and $\boldsymbol{k}_{\rho i} = \hat{\boldsymbol{\rho}}_i k_{\rho i}$ with $k_{\rho i} = k_0 \sin\vartheta_i$. Here $0 \le \vartheta_i < \pi/2$ and

$$\boldsymbol{k}_{\rho i} \cdot \boldsymbol{\rho} = k_0 \sin\vartheta_i\, (x \cos\varphi_i + y \sin\varphi_i) \tag{119}$$

Note that the directions of the unit vectors $\hat{\boldsymbol{\rho}}_i$ and $\hat{\boldsymbol{\varphi}}_i$ are fixed by the angle φ_i, which specifies the *plane of incidence*. Our goal is to find the impressed field $(\boldsymbol{E}^i, \boldsymbol{H}^i)$ established at any point in the layered medium as a result of the plane-wave (118) incident in the upper half-space, which is assumed to be filled with air.

For the fields to match at the interfaces, the dependence of $(\boldsymbol{E}^i, \boldsymbol{H}^i)$ on the transverse coordinates must be the same in all layers and must match that of the incident plane wave (118). Furthermore, both the incident field and the impressed field must satisfy the source-free forms of (14)-(17) with $\boldsymbol{k}_\rho = \boldsymbol{k}_{\rho i}$. Consequently, the transmission-line analog of the layered medium developed in the previous sections may be employed to find $(\boldsymbol{E}^i, \boldsymbol{H}^i)$. In view of (19), where now $(\hat{\boldsymbol{u}}, \hat{\boldsymbol{v}}) = (\hat{\boldsymbol{\rho}}_i, \hat{\boldsymbol{\varphi}}_i)$, we express the transverse part of (118) as

$$\boldsymbol{E}^i_{0t} = \left(\hat{\boldsymbol{\rho}}_i \overleftarrow{V}^e + \hat{\boldsymbol{\varphi}}_i \overleftarrow{V}^h\right) e^{-j\boldsymbol{k}_{\rho i}\cdot\boldsymbol{\rho}} \tag{120}$$

where

$$\overleftarrow{V}^e = E_0 \cos\zeta_i \cos\vartheta_i \, e^{jk_{zi}(z-z_0)}, \quad \overleftarrow{V}^h = E_0 \sin\zeta_i \, e^{jk_{zi}(z-z_0)} \tag{121}$$

We may interpret $\overleftarrow{V}^e$ and $\overleftarrow{V}^h$ are the leftward propagating *incident* voltage waves exciting the TM and TE transmission-line networks, respectively, in the line section corresponding to the upper-half-space. In view of (24)-(25), the impressed fields in any layer may now be found as

$$\boldsymbol{E}^i = \left(\hat{\boldsymbol{\rho}}_i V^e + \hat{\boldsymbol{\varphi}}_i V^h - \hat{\boldsymbol{z}} \frac{\eta_0}{\epsilon_z} \sin\vartheta_i \, I^e\right) e^{-j\boldsymbol{k}_{\rho i}\cdot\boldsymbol{\rho}} \tag{122}$$

$$\boldsymbol{H}^i = \left(-\hat{\boldsymbol{\rho}}_i I^h + \hat{\boldsymbol{\varphi}}_i I^e + \hat{\boldsymbol{z}} \frac{1}{\eta_0\mu_z} \sin\vartheta_i \, V^h\right) e^{-j\boldsymbol{k}_{\rho i}\cdot\boldsymbol{\rho}} \tag{123}$$

where $V^p(z)$ and $I^p(z)$ are the *total* voltage and current at a point z on the transmission-line network. If the uppermost interface is at z_n, the total voltage and current on the transmission-line section n corresponding to the upper half-space are found as

$$V^p(z) = \overleftarrow{V}^p(z) \, \overleftarrow{\tau}^p_n(z), \quad I^p(z) = \overleftarrow{V}^p(z) \, \overleftarrow{\mathcal{Y}}^p_n(z) \tag{124}$$

In any other line section m, $V^p(z)$ and $I^p(z)$ are given by (87), where $V^p(z_n)$ is computed via (124). All transmission-line voltages and currents in the above are evaluated with $k_\rho = k_{\rho i}$.

With reference to Fig. 8, observe that the polarization of the incident plane wave is parallel for $\zeta_i = 0$, and perpendicular for $\zeta_i = \pi/2$. >From (121) we see that the parallel- and perpendicularly polarized waves only excite the TM and TE transmission-lines, respectively, and that both lines are excited by an arbitrarily polarized wave. In the case of normal incidence, the field is TEM and the plane of incidence, and thus also φ_i and ζ_i, are undefined. However, this situation may be treated as a limiting case of parallel or perpendicular polarization as $\vartheta_i \to 0$.

XI Summary and Conclusion

A compact and efficient formulation is presented of the electric- and magnetic-type dyadic Green's functions (DGFs) for plane-stratified, multilayered uniaxial media, based on the transmission-line network analog along the axis normal to the stratification [75]. Within the

framework of this transmission-line formalism, mixed-potential integral equations (MPIEs) are derived for arbitrarily shaped, conducting or penetrable objects embedded in a the layered medium. The DGFs and the MPIE kernels are expressed in terms of four transmission-line Green's functions (TLGFs), which are the voltages and currents on the transmission-line network excited by unit-strength series voltage of shunt current sources. A practical algorithm is given for the efficient computation of the TLGFs. Although the development emphasizes laterally unbounded configurations, an extension to the important case of a layered medium enclosed by a rectangular shield is also presented. Some important practical issues encountered in the computation of the spectral integrals and series that arise in the MPIE kernels are discussed. Finally, the far-zone field and the plane-wave impressed field in the layered medium are also derived in terms of the TLGFs.

The unified formulation presented here is elegant and computationally efficient, and it affords much insight into the various Green's functions and kernels, because the behavior of the transmission-line voltages and currents—which are governed by the simple telegraphist's equations—is well understood. The MPIEs derived here should be particularly useful in the analysis of inhomogeneities—such as mines—buried in layered earth, and in the modeling of integrated dielectric waveguides and high-speed digital interconnects, as well as probe-fed and aperture-coupled microstrip patch antennas and arrays, and complex microwave integrated circuits—including those comprising vertical transitions, air-bridges, and vias.

There has been a definite trend recently to use the MPIEs, even for strictly planar microstrip structures. Among integral equation formulations, the space-domain MPIE approach is—in our experience—the *only viable way* to analyze complex three-dimensional objects embedded in multilayered media.

Acknowledgment

The authors acknowledge with gratitude many personal communications regarding the subject of this paper with Donald R. Wilton of the University of Houston, Texas.

References

[1] A. Karlsson and G. Kristensson, "Electromagnetic scattering from subterranean obstacles in a stratified ground," *Radio Sci.*, vol. 18, pp. 345–356, May-June 1983.

[2] P. E. Wannamaker, G. W. Hohmann, and W. A. SanFilipo, "Electromagnetic modeling of three-dimensional bodies in layered earths using integral equations," *Geophys.*, vol. 49, pp. 60–74, Jan. 1984.

[3] R. H. Hardman and L. C. Shen, "Theory of induction sonde in dipping beds," *Geophys.*, vol. 51, pp. 800–809, Mar. 1986.

[4] L. Tsang, E. Njoku, and J. A. Kong, "Microwave thermal emission from a stratified medium with nonuniform temperature distribution," *J. Appl. Phys.*, vol. 46, pp. 5127–5133, Dec. 1975.

[5] J. R. Wait, *Wave Propagation Theory*. New York: Pergamon Press, 1981.

[6] G. P. S. Cavalcante, D. A. Rogers, and A. J. Giarola, "Analysis of electromagnetic wave propagation in multilayered media using dyadic Green's functions," *Radio Sci.*, vol. 17, pp. 503–508, May-June 1982.

[7] W. P. Harokopus and P. B. Katehi, "Radiation losses in microstrip antenna feed networks printed on multilayer substrates," *Int. J. Num. Mod.*, vol. 4, pp. 3–18, 1991.

[8] N. Faché, F. Olyslager, and D. De Zutter, *Electromagnetic and Circuit Modelling of Multiconductor Transmission Lines*. Oxford: Clarendon Press, 1993.

[9] A. K. Bhattacharyya, *Electromagnetic Fields in Multilayered Structures*. Boston: Artech House, 1994.

[10] S. M. Ali and S. F. Mahmoud, "Electromagnetic fields of buried sources in stratified anisotropic media," *IEEE Trans. Antennas Propagat.*, vol. AP–27, pp. 671–678, Sept. 1979.

[11] J. K. Lee and J. A. Kong, "Dyadic Green's functions for layered anisotropic medium," *Electromagn.*, vol. 3, pp. 111–130, 1983.

[12] T. Sphicopoulos, V. Teodoridis, and F. E. Gardiol, "Dyadic Green function for the electromagnetic field in multilayered isotropic media: An operator approach," *IEE Proc., Pt. H*, vol. 132, pp. 329–334, Aug. 1985.

[13] J. S. Bagby, D. P. Nyquist, and B. C. Drachman, "Integral formulation for analysis of integrated dielectric waveguides," *IEEE Trans. Microwave Theory Tech.*, vol. MTT-33, pp. 906–915, Oct. 1985.

[14] D. H. S. Cheng, "On the formulation of the dyadic Green's function in a layered medium," *Electromagn.*, vol. 6, no. 2, pp. 171–182, 1986.

[15] C. M. Krowne, "Determination of the Green's function in the spectral domain using a matrix method: Application to radiators immersed in a complex anisotropic layered medium," *IEEE Trans. Antennas Propagat.*, vol. AP–34, pp. 247–253, Feb. 1986.

[16] N. K. Das and D. M. Pozar, "A generalized spectral-domain Green's function for multilayer dielectric substrates with application to multilayer transmission lines," *IEEE Trans. Microwave Theory Tech.*, vol. MTT-35, pp. 326–335, Mar. 1987.

[17] L. Beyne and D. De Zutter, "Green's function for layered lossy media with special application to microstrip antennas," *IEEE Trans. Microwave Theory Tech.*, vol. 36, pp. 875–881, May 1988.

[18] L. Vegni, R. Cicchetti, and P. Capece, "Spectral dyadic Green's function formulation for planar integrated structures," *IEEE Trans. Antennas Propagat.*, vol. 36, pp. 1057–1065, Aug. 1988.

[19] R. Kastner, E. Heyman, and A. Sabban, "Spectral domain iterative analysis of single- and double-layered microstrip antennas using the conjugate gradient algorithm," *IEEE Trans. Antennas Propagat.*, vol. 36, pp. 1204–1212, Sept. 1988.

[20] E. W. Kolk, N. H. G. Baken, and H. Blok, "Domain integral equation analysis of integrated optical channel and ridge waveguides in stratified media," *IEEE Trans. Microwave Theory Tech.*, vol. 38, pp. 78–85, Jan. 1990.

[21] J. F. Kiang, S. M. Ali, and J. A. Kong, "Integral equation solution to the guidance and leakage properties of coupled dielectric strip waveguides," *IEEE Trans. Microwave Theory Tech.*, vol. 38, pp. 193–203, Feb. 1990.

[22] T. M. Habashy, S. M. Ali, J. A. Kong, and M. D. Grossi, "Dyadic Green's functions in a planar, stratified, arbitrarily magnetized linear plasma," *Radio Sci.*, vol. 26, pp. 701–715, May-June 1991.

[23] S. M. Ali, T. M. Habashy, and J. A. Kong, "Spectral-domain dyadic Green's function in layered chiral media," *J. Opt. Soc. Am. A*, vol. 9, pp. 413–423, Mar. 1992.

[24] S. Barkeshli and P. H. Pathak, "On the dyadic Green's function for a planar multilayered dielectric/magnetic media," *IEEE Trans. Microwave Theory Tech.*, vol. 40, pp. 128–142, Jan. 1992.

[25] H. J. M. Bastiaansen, N. H. G. Baken, and H. Blok, "Domain-integral analysis of channel waveguides in anisotropic multi-layered media," *IEEE Trans. Microwave Theory Tech.*, vol. 40, pp. 1918–1926, Oct. 1992.

[26] S. Barkeshli, "On the electromagnetic dyadic Green's functions for planar multilayered anisotropic uniaxial material media," *Int. J. Infrared Millimeter Waves*, vol. 13, no. 4, pp. 507–527, 1992.

[27] P. Bernardi and R. Cicchetti, "Dyadic Green's functions for conductor-backed layered structures excited by arbitrary tridimensional sources," *IEEE Trans. Microwave Theory Tech.*, vol. 42, pp. 1474–1483, Aug. 1994.

[28] S.-G. Pan and I. Wolff, "Scalarization of dyadic spectral Green's functions and network formalism for three-dimensional full-wave analysis of planar lines and antennas," *IEEE Trans. Microwave Theory Tech.*, vol. 42, pp. 2118–2127, Nov. 1994.

[29] A. Dreher, "A new approach to dyadic Green's function in spectral domain," *IEEE Trans. Antennas Propagat.*, vol. 43, pp. 1297–1302, Nov. 1995.

[30] R. F. Harrington, *Field Computation by Moment Methods*. New York: Macmillan, 1968. Reprinted by Krieger Publishing Co., Melbourne, FL, 1982.

[31] J. C. Chao, Y. J. Liu, F. J. Rizzo, P. A. Martin, and L. Udpa, "Regularized integral equations for curvilinear boundary elements for electromagnetic wave scattering in three dimensions," *IEEE Trans. Antennas Propagat.*, vol. 43, pp. 1416–1422, Dec. 1995.

[32] A. W. Glisson and D. R. Wilton, "Simple and efficient numerical methods for problems of electromagnetic radiation and scattering from surfaces," *IEEE Trans. Antennas Propagat.*, vol. AP-28, pp. 593–603, Sept. 1980.

[33] S. M. Rao, D. R. Wilton, and A. W. Glisson, "Electromagnetic scattering by surfaces of arbitrary shape," *IEEE Trans. Antennas Propagat.*, vol. AP-30, pp. 409–418, May 1982.

[34] D. H. Schaubert, D. R. Wilton, and A. W. Glisson, "A tetrahedral modeling method for electromagnetic scattering by arbitrarily shaped inhomogeneous dielectric bodies," *IEEE Trans. Antennas Propagat.*, vol. AP-32, pp. 77–85, Jan. 1984.

[35] K. Umashankar, A. Taflove, and S. M. Rao, "Electromagnetic scattering by arbitrary shaped three-dimensional homogeneous lossy dielectric objects," *IEEE Trans. Antennas Propagat.*, vol. AP-34, pp. 758–766, June 1986.

[36] J. R. Mosig and F. E. Gardiol, "A dynamical radiation model for microstrip structures," in *Adv. Electron. Electron Phys.* (P. W. Hawkes, ed.), vol. 59, pp. 139–237, New York: Academic Press, 1982.

[37] J. R. Mosig and F. E. Gardiol, "Analytic and numerical techniques in the Green's function treatment of microstrip antennas and scatterers," *IEE Proc., Pt. H*, vol. 130, pp. 175–182, Mar. 1983.

[38] J. R. Mosig and F. E. Gardiol, "General integral equation formulation for microstrip antennas and scatterers," *IEE Proc., Pt. H*, vol. 132, pp. 424–432, Dec. 1985.

[39] K. A. Michalski, "The mixed-potential electric field integral equation for objects in layered media," *Arch. Elek. Übertragung.*, vol. 39, pp. 317–322, Sept.–Oct. 1985.

[40] K. A. Michalski, "On the scalar potential of a point charge associated with a time-harmonic dipole in a layered medium," *IEEE Trans. Antennas Propagat.*, vol. AP-35, pp. 1299–1301, Nov. 1987.

[41] R. C. Hall and J. R. Mosig, "The analysis of coaxially fed microstrip antennas with electrically thick substrates," *Electromagn.*, vol. 9, no. 4, pp. 367–384, 1989.

[42] J. R. Mosig, "Integral equation technique," in *Numerical Techniques for Microwave and Millimeter–Wave Passive Structures* (T. Itoh, ed.), pp. 133–213, New York: Wiley, 1989.

[43] J. R. Mosig, R. C. Hall, and F. E. Gardiol, "Numerical analysis of microstrip patch antennas," in *Handbook of Microstrip Antennas* (J. R. James and P. S. Hall, eds.), pp. 391–453, London: Peter Peregrinus, 1989.

[44] H. Legay, R. Gillard, J. Citerne, and G. Piton, "Via-hole effects on radiation characteristics of a patch microstrip antenna coaxially fed through the ground plane," *Ann. Télécommun.*, vol. 46, no. 7-8, pp. 367–381, 1991.

[45] D. Zheng and K. A. Michalski, "Analysis of arbitrarily shaped coax-fed microstrip antennas—A hybrid mixed-potential integral equation approach," *Microwave & Opt. Technol. Lett.*, vol. 3, pp. 200–203, June 1990.

[46] G. A. E. Vandenbosch and A. R. Van de Capelle, "Mixed-potential integral expression formulation of the electric field in a stratified dielectric medium—Application to the case of a probe current source," *IEEE Trans. Antennas Propagat.*, vol. 40, pp. 806–817, July 1992.

[47] P. Pichon, J. R. Mosig, and A. Papiernik, "Input impedance of arbitrarily shaped microstrip antennas," *Electron. Lett.*, vol. 24, pp. 1214–1215, Sept. 1988.

[48] W. Wertgen and R. H. Jansen, "Efficient direct and iterative electrodynamic analysis of geometrically complex MIC and MMIC structures," *Int. J. Num. Mod.*, vol. 2, pp. 153–186, 1989.

[49] L. Barlatey, J. R. Mosig, and T. Sphicopoulos, "Analysis of stacked microstrip patches with a mixed potential integral equation," *IEEE Trans. Antennas Propagat.*, vol. 38, pp. 608–615, May 1990.

[50] K.-L. Wu, J. Litva, R. Fralich, and C. Wu, "Full-wave analysis of arbitrarily shaped line-fed microstrip antennas using triangular finite-element method," *IEE Proc., Pt. H*, vol. 138, pp. 421–428, Oct. 1991.

[51] A. Hoorfar, J. X. Zheng, and D. C. Chang, "Numerical modeling of crossover and other junction discontinuities in two-layer microstrip circuits," *Int. J. Microwave Millimeter-Wave Computer-Aided Eng.*, vol. 2, no. 4, pp. 261–272, 1992.

[52] F. Alonso-Monferrer, A. A. Kishk, and A. W. Glisson, "Green's function analysis of planar circuits in a two-layer grounded medium," *IEEE Trans. Antennas Propagat.*, vol. 40, pp. 690–696, June 1992.

[53] L. Barlatey, H. Smith, and J. Mosig, "Printed radiating structures and transitions in multilayered substrates," *Int. J. Microwave Millimeter-Wave Computer-Aided Eng.*, vol. 2, no. 4, pp. 273–285, 1992.

[54] T. K. Sarkar, P. Midya, Z. A. Maricevic, M. Kahrizi, S. M. Rao, and A. R. Djordjevic, "Analysis of arbitrarily shaped microstrip patch antennas using the Sommerfeld formulation," *Int. J. Microwave Millimeter-Wave Computer-Aided Eng.*, vol. 2, no. 3, pp. 168–178, 1992.

[55] R. D. Cloux, G. P. J. F. M. Maas, and A. J. H. Wachters, "Quasi-static boundary element method for electromagnetic simulation of PCBS," *Philips J. Res.*, vol. 48, no. 1–2, pp. 117–144, 1994.

[56] J. Sercu, N. Faché, F. Libbrecht, and P. Lagasse, "Mixed potential integral equation technique for hybrid microstrip-slotline multilayered circuits using a mixed rectangular-triangular mesh," *IEEE Trans. Microwave Theory Tech.*, vol. 43, pp. 1162–1172, May 1995.

[57] L. Giauffret and J.-M. Laheurte, "Theoretical and experimental characterization of CPW-fed microstrip antennas," *IEE Proc.-Microw. Antennas Propag.*, vol. 143, pp. 13–17, Feb. 1996.

[58] K. A. Michalski and D. Zheng, "Electromagnetic scattering and radiation by surfaces of arbitrary shape in layered media, Part I: Theory," *IEEE Trans. Antennas Propagat.*, vol. 38, pp. 335–344, Mar. 1990.

[59] K. A. Michalski and D. Zheng, "Electromagnetic scattering and radiation by surfaces of arbitrary shape in layered media, Part II: Implementation and results for contiguous half-spaces," *IEEE Trans. Antennas Propagat.*, vol. 38, pp. 345–352, Mar. 1990.

[60] W. A. Johnson, "Analysis of vertical, tubular cylinder which penetrates an air-dielectric interface and which is excited by an azimuthally symmetric source," *Radio Sci.*, vol. 18, pp. 1273–1281, Nov.-Dec. 1983.

[61] K. A. Michalski, C. E. Smith, and C. M. Butler, "Analysis of a horizontal two-element array antenna above a dielectric halfspace," *IEE Proc., Pt. H*, vol. 132, pp. 335–338, Aug. 1985.

[62] S. Singh and D. R. Wilton, "Analysis of an infinite periodic array of slot radiators with dielectric loading," *IEEE Trans. Antennas Propagat.*, vol. 39, pp. 190–196, Feb. 1991.

[63] K. A. Michalski and D. Zheng, "Rigorous analysis of open microstrip lines of arbitrary cross section in bound and leaky regimes," *IEEE Trans. Microwave Theory Tech.*, vol. 37, pp. 2005–2010, Dec. 1989.

[64] D. Zheng and K. A. Michalski, "Analysis of coaxially fed microstrip antennas of arbitrary shape with thick substrates," *J. Electromagn. Waves Appl.*, vol. 5, no. 12, pp. 1303–1327, 1991.

[65] K. A. Michalski and D. Zheng, "Analysis of microstrip resonators of arbitrary shape," *IEEE Trans. Antennas Propagat.*, vol. 40, pp. 112–119, Jan. 1992.

[66] N. J. Champagne, J. T. Williams, and D. R. Wilton, "Analysis of resistively loaded, printed spiral antennas," *Electromagn.*, vol. 14, pp. 363–395, July-Dec. 1994.

[67] N. W. Montgomery and D. R. Wilton, "Analysis of arbitrary conducting periodic structures embedded in layered media," in *Digest IEEE AP-S Int. Symp.*, (London, Ontario), pp. 1889–1892, June 1991.

[68] D. R. Wilton, "Review of current status and trends in the use of integral equations in computational electromagnetics," *Electromagn.*, vol. 12, pp. 287–341, July-Dec. 1992.

[69] J. Chen, A. A. Kishk, and A. W. Glisson, "MPIE for conducting sheets penetrating a multilayer medium," in *Digest IEEE AP-S Int. Symp.*, (Seattle, WA), pp. 1346–1349, June 1994.

[70] K. A. Michalski, "Mixed-potential integral equation (MPIE) formulation for nonplanar microstrip structures of arbitrary shape in multilayered uniaxial media," *Int. J. Microwave Millimeter-Wave Computer-Aided Eng.*, vol. 3, no. 4, pp. 420–431, 1993.

[71] K. A. Michalski, "Formulation of mixed-potential integral equations for arbitrarily shaped microstrip structures with uniaxial substrates," *J. Electromagn. Waves Appl.*, vol. 7, no. 7, pp. 899–917, 1993.

[72] S. Vitebskiy and L. Carin, "Moment method modeling of short-pulse scattering from and the resonances of a wire buried inside a lossy, dispersive half-space," *IEEE Trans. Antennas Propagat.*, vol. 43, pp. 1303–1312, Nov. 1995.

[73] A. Abdelmageed, K. A. Michalski, and A. W. Glisson, "Analysis of EM scattering by conducting bodies of revolution in layered media using the discrete complex image method," in *Digest IEEE AP-S Int. Symp.*, (Newport Beach, CA), pp. 402–406, June 1995.

[74] S. Vitebskiy, K. Sturgess, and L. Carin, "Short-pulse plane-wave scattering from buried perfectly conducting bodies of revolution," *IEEE Trans. Antennas Propagat.*, vol. 44, pp. 143–151, Feb. 1996.

[75] L. B. Felsen and N. Marcuvitz, *Radiation and Scattering of Waves*. Englewood Cliffs, N.J.: Prentice Hall, 1973.

[76] N. G. Alexopoulos, "Integrated-circuit structures on anisotropic substrates," *IEEE Trans. Microwave Theory Tech.*, vol. MTT-33, pp. 847–881, Oct. 1985.

[77] D. M. Pozar, "Radiation and scattering from a microstrip patch on a uniaxial substrate," *IEEE Trans. Antennas Propagat.*, vol. AP-35, pp. 613–621, June 1987.

[78] Z. Xiong, Y. Luo, S. Wang, and G. Wu, "Induced-polarization and electromagnetic modeling of a three-dimensional body buried in a two-layer anisotropic earth," *Geophys.*, vol. 51, pp. 2235–2246, Dec. 1986.

[79] R. F. Harrington, *Time-Harmonic Electromagnetic Field*. New York: McGraw-Hill, 1961.

[80] J. Van Bladel, *Electromagnetic Fields*. New York: Hemisphere, 1985.

[81] A. J. Poggio and E. K. Miller, "Integral equation solutions of three-dimensional scattering problems," in *Computer Techniques for Electromagnetics* (R. Mittra, ed.), ch. 4, New York: Pergamon Press, 1973.

[82] R. F. Harrington, "The method of moments in electromagnetics," *J. Electromagn. Waves Appl.*, vol. 1, no. 3, pp. 181–200, 1987.

[83] A. A. Sebak and L. Shafai, "Performance of various integral equation formulations for numerical solution of scattering by impedance objects," *Can. J. Phys.*, vol. 62, pp. 605–615, 1984.

[84] A. W. Glisson, "Electromagnetic scattering by arbitrarily shaped surfaces with impedance boundary conditions," *Radio Sci.*, vol. 27, pp. 935–943, Nov.-Dec. 1992.

[85] I. P. Theron and J. H. Cloete, "On the surface impedance used to model the conductor losses of microstrip structures," *IEE Proc.-Microw. Antennas Propag.*, vol. 142, pp. 35–40, Feb. 1995.

[86] R. F. Harrington, "Boundary integral formulations for homogeneous material bodies," *J. Electromagn. Waves Appl.*, vol. 3, no. 1, pp. 1–15, 1989.

[87] K. H. Lee, D. F. Pridmore, and H. F. Morrison, "A hybrid three-dimensional electromagnetic modeling scheme," *Geophys.*, vol. 46, pp. 796–805, May 1981.

[88] J. Wu and K. A. Michalski, "Hybrid finite element – mixed-potential integral equation–discrete complex image approach for inhomogeneous waveguides in layered media," in *Digest IEEE AP-S Int. Symp.*, (Newport Beach, CA), pp. 1472–1475, June 1995.

[89] T. F. Eibert and V. Hansen, "FEM/BEM-hybrid approach for layered media," in *Digest IEEE AP-S Int. Symp.*, (Newport Beach, CA), pp. 1464–1467, June 1995.

[90] T. F. Eibert and V. Hansen, "3D FEM/BEM-hybrid approach for planar layered media," *Electromagn.*, to appear.

[91] X.-B. Xu and W. Yan, "Modification of hybrid integral equations for determining scattering by an inhomogeneous cylinder of discontinuous electromagnetic parameters near a media interface," *J. Electromagn. Waves Appl.*, vol. 7, no. 10, pp. 1389–1394, 1993.

[92] C. M. Butler, Y. Rahmat-Samii, and R. Mittra, "Electromagnetic penetration through apertures in conducting surfaces," *IEEE Trans. Antennas Propagat.*, vol. AP-26, pp. 82–93, Jan. 1978.

[93] W. A. Johnson, D. R. Wilton, and R. M. Sharpe, "Modeling scattering from and radiation by arbitrarily shaped objects with the electric field integral equation triangular surface patch code," *Electromagn.*, vol. 10, no. 1-2, pp. 41–63, 1990.

[94] T. Itoh, "Spectral-domain immittance approach for dispersion characteristics of generalized printed transmission lines," *IEEE Trans. Microwave Theory Tech.*, vol. MTT-28, pp. 733–736, July 1980.

[95] W. C. Chew and Q. Liu, "Resonance frequency of a rectangular microstrip patch," *IEEE Trans. Antennas Propagat.*, vol. 36, pp. 1045–1056, Aug. 1988.

[96] T.-S. Horng, N. G. Alexopoulos, S.-C. Wu, and H.-Y. Yang, "Full-wave spectral analysis for open microstrip discontinuities of arbitrary shape including radiation and surface-wave losses," *Int. J. Microwave Millimeter-Wave Computer-Aided Eng.*, vol. 2, no. 4, pp. 224–240, 1992.

[97] T. Becks and I. Wolff, "Analysis of 3–D metallization structures by a full-wave spectral domain technique," *IEEE Trans. Microwave Theory Tech.*, vol. 40, pp. 2219–2227, Dec. 1992.

[98] K. A. Michalski and D. Zheng, "Analysis of planar microstrip structures of arbitrary shape—To be, or not to be in the spectral domain?," in *Proc. Symp. on Antenna Techn. and Appl. Electromagn.*, (Winnipeg, Canada), pp. 240–245, Aug. 1990.

[99] A. Sommerfeld, *Partial Differential Equations in Physics*. New York: Academic Press, 1949.

[100] C.-I. G. Hsu, R. F. Harrington, K. A. Michalski, and D. Zheng, "Analysis of a multiconductor transmission lines of arbitrary cross-section in multilayered uniaxial media," *IEEE Trans. Microwave Theory Tech.*, vol. 41, pp. 70–78, Jan. 1993.

[101] W. C. Chew, *Waves and Fields in Inhomogeneous Media*. New York: Van Nostrand Reinhold, 1990.

[102] G. J. Burke, E. K. Miller, J. N. Brittingham, D. L. Lager, R. J. Lytle, and J. T. Okada, "Computer modeling of antennas near the ground," *Electromagn.*, vol. 1, pp. 29–49, Jan.-Mar. 1981.

[103] K. A. Michalski, "On the efficient evaluation of integrals arising in the Sommerfeld halfspace problem," in *Moment Methods in Antennas and Scatterers* (R. C. Hansen, ed.), pp. 325–331, Boston: Artech House, 1990.

[104] E. H. Newman and D. Forrai, "Scattering from a microstrip patch," *IEEE Trans. Antennas Propagat.*, vol. AP-35, pp. 245–251, Mar. 1987.

[105] L. T. Hildebrand and D. A. McNamara, "A guide to implementation aspects of the spatial-domain integral equation analysis of microstrip antennas," *Appl. Comput. Electromagn. Soc. J.*, vol. 10, no. 1, pp. 40–51, 1995.

[106] A. D. Chave, "Numerical integration of related Hankel transforms by quadrature and continued fraction expansion," *Geophys.*, vol. 48, pp. 1671–1686, Dec. 1983.

[107] R. A. Kipp and C. H. Chan, "Complex image method for sources in bounded regions of multilayer structures," *IEEE Trans. Microwave Theory Tech.*, vol. 42, pp. 860–865, May 1994.

[108] D. G. Fang, J. J. Yang, and G. Y. Delisle, "Discrete image theory for horizontal electric dipoles in a multilayered medium," *IEE Proc., Pt. H*, vol. 135, pp. 297–303, Oct. 1988.

[109] Y. L. Chow, J. J. Yang, D. G. Fang, and G. E. Howard, "A closed-form spatial Green's function for the thick microstrip substrate," *IEEE Trans. Microwave Theory Tech.*, vol. 39, pp. 588–592, Mar. 1991.

[110] M. I. Aksun and R. Mittra, "Derivation of closed-form Green's functions for a general microstrip geometry," *IEEE Trans. Microwave Theory Tech.*, vol. 40, pp. 2055–2062, Nov. 1992.

[111] G. Dural and M. I. Aksun, "Closed-form Green's functions for general sources in stratified media," *IEEE Trans. Microwave Theory Tech.*, vol. 43, pp. 1545–1552, July 1995.

[112] M. I. Aksun, "A robust approach for the derivation of closed-form Green's functions," *IEEE Trans. Microwave Theory Tech.*, vol. 44, pp. 651–658, May 1996.

[113] K. A. Michalski and J. R. Mosig, "Discrete complex image mixed-potential integral equation analysis of coax-fed coupled vertical monopoles in a grounded dielectric substrate: Two formulations," *IEE Proc.-Microw. Antennas Propag.*, vol. 142, pp. 269–274, June 1995.

[114] T. K. Sarkar and O. Pereira, "Using the matrix pencil method to estimate the parameters of a sum of complex exponentials," *IEEE Antennas Propagat. Magaz.*, vol. 37, pp. 48–55, Feb. 1995.

[115] K. A. Michalski and J. R. Mosig, "Discrete complex image mixed-potential integral equation analysis of microstrip patch antennas with vertical probe feeds," *Electromagn.*, vol. 15, pp. 377–392, July-Aug. 1995.

[116] L.-W. Li, P.-S. Kooi, M.-S. Leong, T.-S. Yeo, and S.-L. Ho, "Input impedance of probe-excited semi-infinite rectangular waveguide with arbitrary multilayered loads: Part I—Dyadic Green's functions," *IEEE Trans. Microwave Theory Tech.*, vol. 43, pp. 1559–1566, July 1995.

[117] A. Hill, J. Burke, and K. Kottapalli, "Three-dimensional electromagnetic analysis of shielded microstrip circuits," *Int. J. Microwave Millimeter-Wave Computer-Aided Eng.*, vol. 2, no. 4, pp. 286–296, 1992.

[118] R. W. Jackson, "The use of side images to compute package effects in MoM analysis of MMIC circuits," *IEEE Trans. Microwave Theory Tech.*, vol. 41, pp. 406–414, Mar. 1993.

[119] A. Papoulis, *The Fourier Integral and its Applications.* New York: McGraw-Hill, 1962.

[120] M.-H. Ho, K. A. Michalski, and K. Chang, "Waveguide excited microstrip patch antenna – Theory and experiment," *IEEE Trans. Antennas Propagat.*, vol. 42, pp. 1114–1125, Aug. 1994.

[121] K. E. Jordan, G. R. Richter, and P. Sheng, "An efficient numerical evaluation of the Green's function for the Helmholtz operator on periodic structures," *J. Comput. Phys.*, vol. 63, pp. 222–235, 1986.

[122] E. Cohen, "Critical distance for grating lobe series," *IEEE Trans. Antennas Propagat.*, vol. 39, pp. 677–679, May 1991.

[123] S. Singh, W. F. Richards, J. R. Zinecker, and D. R. Wilton, "Accelerating the convergence of series representing the free space periodic Green's function," *IEEE Trans. Antennas Propagat.*, vol. 38, pp. 1958–1962, Dec. 1990.

[124] R. M. Shubair and Y. L. Chow, "Efficient computation of the periodic Green's function in layered media," *IEEE Trans. Microwave Theory Tech.*, vol. 41, pp. 498–502, Mar. 1993.

[125] J. Xu, “Fast convergent dyadic Green’s function in a rectangular waveguide,” *Int. J. Infrared Millimeter Waves*, vol. 14, no. 9, pp. 1789–1800, 1993.

[126] G. V. Eleftheriades, J. R. Mosig, and M. Gugliemi, “A fast integral equation technique for shielded planar circuits defined on non-uniform meshes,” *IEEE Trans. Microwave Theory Tech.*, to appear.

[127] W. C. Chew, “A quick way to approximate a Sommerfeld-Weyl-type integral,” *IEEE Trans. Antennas Propagat.*, vol. 36, pp. 1654–1657, Nov. 1988.

[128] K. A. Michalski and C.-I. G. Hsu, “RCS computation of coax-loaded microstrip patch antennas of arbitrary shape,” *Electromagn.*, vol. 14, no. 1, pp. 33–63, 1994.

[129] J. R. Mosig and F. E. Gardiol, “Radiation of an arbitrarily shaped microstrip antenna,” *Ann. Télécommun.*, vol. 40, no. 3-4, pp. 181–189, 1985.

TABLE I
CORRESPONDENCE BETWEEN FIELD SOURCES AND TRANSMISSION-LINE SOURCES

	v^e	i^e	v^h	i^h
$\tilde{J}_u$		$\surd$		
$\tilde{J}_v$				$\surd$
$\tilde{J}_z$	$\surd$			
$\tilde{M}_u$			$\surd$	
$\tilde{M}_v$	$\surd$			
$\tilde{M}_z$				$\surd$

TABLE II
ASYMPTOTIC BEHAVIOR OF TRANSMISSION-LINE GREEN'S FUNCTIONS

Green's Function	Asymptotic Behavior
V_i^e, I_v^h	$\mathcal{O}(k_\rho^{+1})$
$V_v^e, I_i^h, V_v^h, I_i^e$	$\mathcal{O}(k_\rho^{0})$
V_i^h, I_v^e	$\mathcal{O}(k_\rho^{-1})$

TABLE III
IMAGE SIGN COEFFICIENTS FOR ELECTRIC SOURCES

Source	s_x	s_y
J_x	$+1$	-1
J_y	-1	$+1$
q, J_z	-1	-1

Figure Captions

Fig. 1. Arbitrarily shaped object in a layered medium. (a) Physical configuration. (b) External equivalent problem.

Fig. 2. Currents radiating in a uniaxial medium. (a) Physical configuration. (b) Transmission-line analog.

Fig. 3. Rotated spectrum-domain coordinate system.

Fig. 4. Network problems for the determination of the transmission-line Green's functions.

Fig. 5. Voltage and current point sources in a transmission-line section.

Fig. 6. Point charge inside a rectangular shield and its images in the $x = 0$ and $y = 0$ PEC planes.

Fig. 7. Geometry for the evaluation of the far-zone field.

Fig. 8. Geometry for the evaluation of the plane-wave incident field.

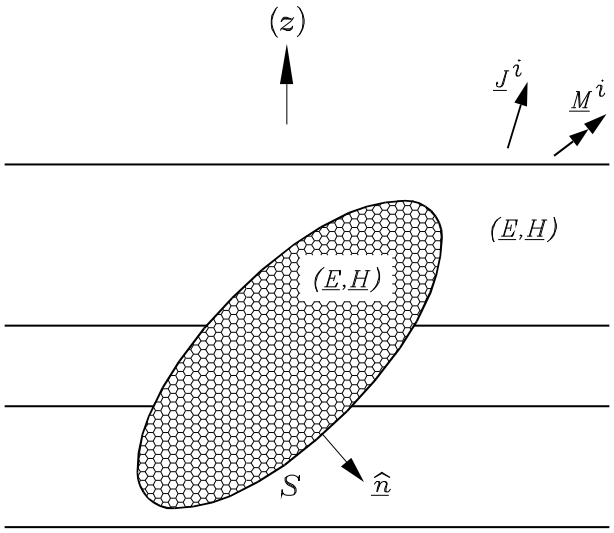
(z)
$\underline{J}^i$
$\underline{M}^i$
$(\underline{E},\underline{H})$
$(\underline{E},\underline{H})$
S
$\hat{\underline{n}}$

(a)

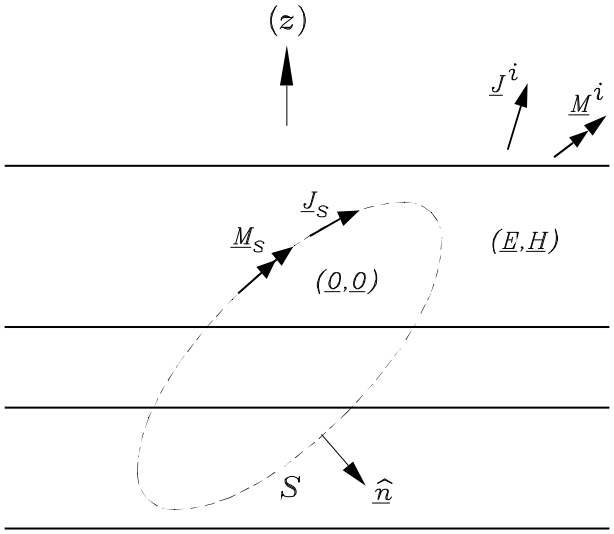
(z)
$\underline{J}^i$
$\underline{M}^i$
$\underline{J}_S$
$\underline{M}_S$
$(\underline{E},\underline{H})$
$(\underline{0},\underline{0})$
S
$\hat{\underline{n}}$

(b)

FIGURE 1

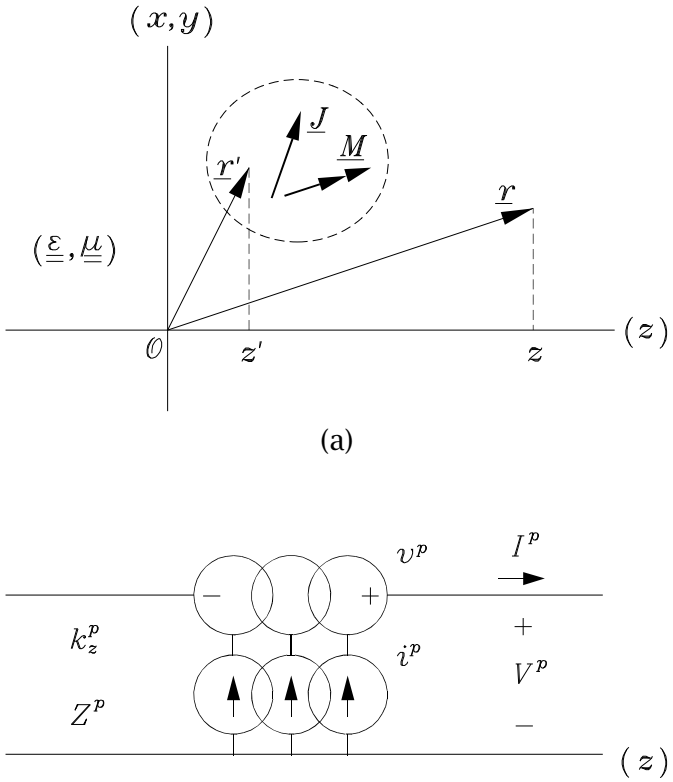
(x,y)
$\underline{J}$
$\underline{M}$
$\underline{r}'$
$\underline{r}$
$(\underline{\underline{\varepsilon}},\underline{\underline{\mu}})$
(z)
0
z'
z
(a)
v^p
I^p
$-$
$+$
$+$
k_z^p
i^p
V^p
Z^p
$-$
(z)
(b)

FIGURE 2

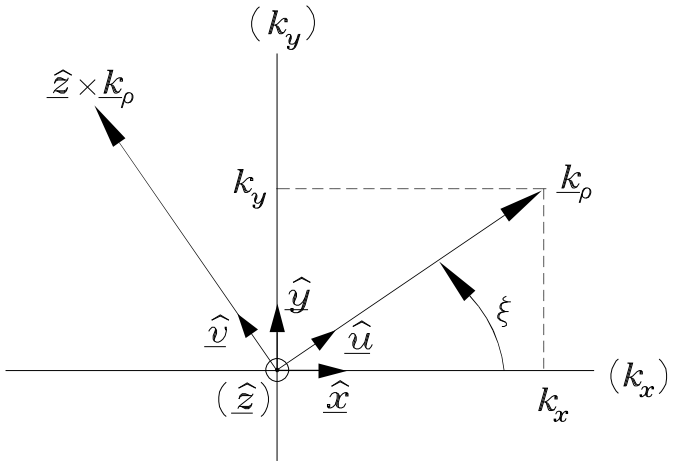
(k_y)
$\hat{\underline{z}} \times \underline{k}_\rho$
k_y
$\underline{k}_\rho$
$\hat{\underline{y}}$
ξ
$\hat{\underline{v}}$
$\hat{\underline{u}}$
(k_x)
$(\hat{\underline{z}})$
$\hat{\underline{x}}$
k_x

FIGURE 3

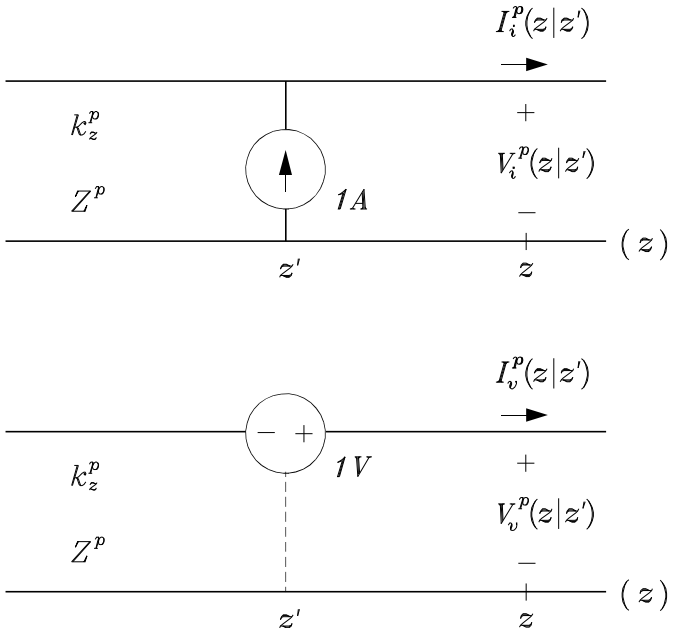

FIGURE 4

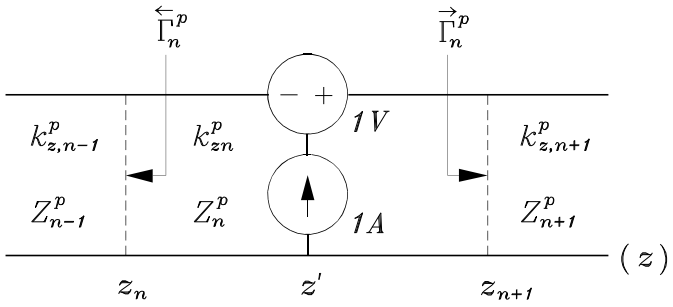
$\overleftarrow{\Gamma}_n^p$
$\overrightarrow{\Gamma}_n^p$
1V
1A
$k_{z,n-1}^p$
k_{zn}^p
$k_{z,n+1}^p$
Z_{n-1}^p
Z_n^p
Z_{n+1}^p
(z)
z_n
z'
z_{n+1}

FIGURE 5

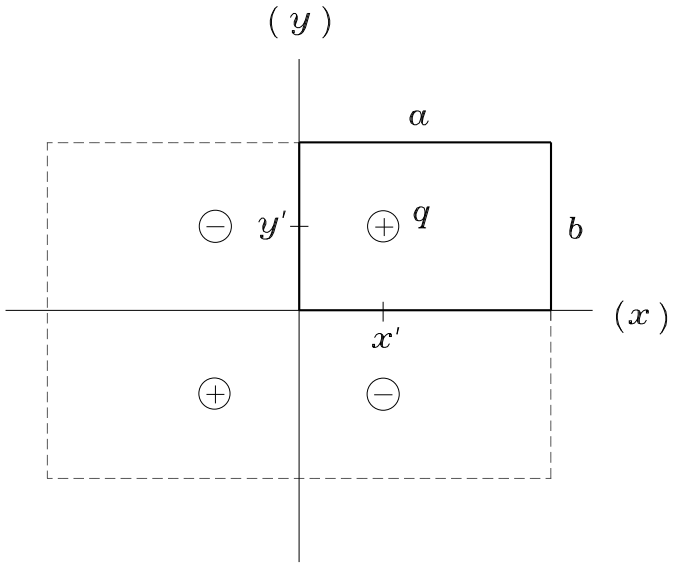

FIGURE 6

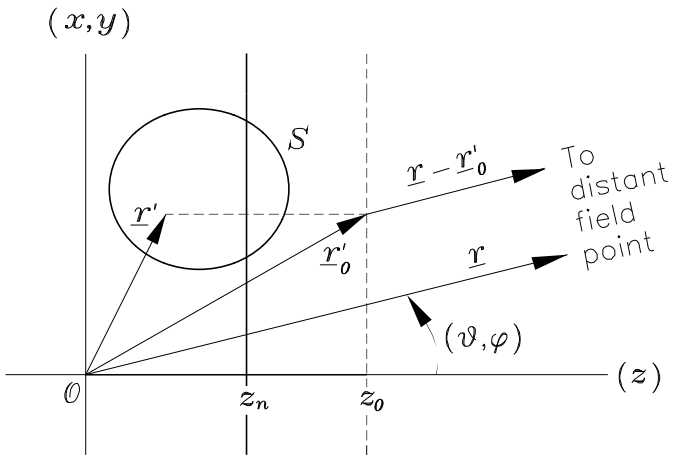
(x,y)
S
$\underline{r}'$
$\underline{r}-\underline{r}'_0$
To distant field point
$\underline{r}'_0$
$\underline{r}$
(ϑ,φ)
(z)
0
z_n
z_0

FIGURE 7

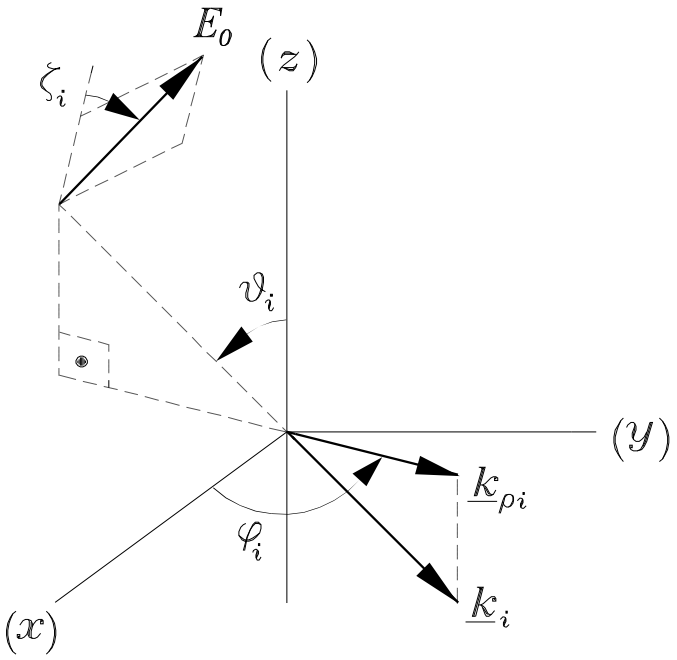
E_0
(z)
ζ_i
ϑ_i
(y)
$\underline{k}_{\rho i}$
φ_i
$\underline{k}_i$
(x)

FIGURE 8